The Continuous Cooling Transformation (CCT) as a Flexible Tool to Investigate Polymer Crystallization under Processing Conditions

ARTICLE *in* ADVANCES IN POLYMER TECHNOLOGY · MARCH 2009

Impact Factor: 1.05 · DOI: 10.1002/adv.20151

4 AUTHORS:

V. Brucato
Università degli Studi di Palermo
59 PUBLICATIONS **688** CITATIONS
SEE PROFILE

Zebene Kiflie
Addis Ababa University
10 PUBLICATIONS **124** CITATIONS
SEE PROFILE

Vincenzo La Carrubba
Università degli Studi di Palermo
101 PUBLICATIONS **367** CITATIONS
SEE PROFILE

Stefano Piccarolo
Università degli Studi di Palermo
116 PUBLICATIONS **1,397** CITATIONS
SEE PROFILE

The Continuous Cooling Transformation (CCT) as a Flexible Tool to Investigate Polymer Crystallization under Processing Conditions

V. BRUCATO, Z. KIFLIE, V. LA CARRUBBA, S. PICCAROLO

Dipartimento di Ingegneria Chimica dei Processi e dei Materiali, Università di Palermo, Viale delle Scienze ed. 6, 90128, Palermo, Italy

Received: January 16, 2009
Accepted: July 6, 2009

ABSTRACT: An experimental route for investigating polymer crystallization over a wide range of cooling rates (from 0.01 to 1000°C/s) and pressures (from 0.1 to 40 MPa) is illustrated, using a method that recalls the approach adopted in metallurgy for studying structure development in metals. Two types of experimental setup were used, namely an apparatus for fast cooling of thin films (100–200 μm thick) at various cooling rates under atmospheric pressure and a device (based on a on-purpose modified injection molding machine) for quenching massive samples (about 1–2 cm^3) under hydrostatic pressure fields. In both cases, ex situ characterization experiments were carried out to probe the resulting structure, using techniques such as density measurements and wide-angle x-ray diffraction (WAXD) patterns. The cooling mechanism and temperature distribution across the sample thickness were analyzed. Results

Correspondence to: V. Brucato; e-mail: vbrucato@dicpm.unipa.it.

Contract grant sponsor: Italian Ministry of research (MURST).
Contract grant number: PRIN 1999.
Contract grant sponsor: UE BRITE.
Contract grant number: BRPRCT960147.

show that the final structure is determined only by the imposed thermal history and pressure. Experimental results for isotactic polypropylene (iPP), poly(ethylene terephthalate) (PET), polyamide 6 (PA6), and syndiotactic polystyrene (sPS) are reported, showing the reliability of this experimental approach to assess not only quantitative information but also a qualitative description of the crystallization behavior of different classes of semicrystalline polymers. The present study gives an opportunity to evaluate how the combined effect of the cooling rate and pressure influences the crystallization kinetics for various classes of polymer of commercial interest. An increase in the cooling rate translates into a decrease in crystallinity and density, which both experience a sudden drop around the specific "crystallizability" (or "critical cooling rate") of the material examined. The exception is sPS where competition among the various crystalline modifications determines a minimum in the plot of density vs. cooling rate. As for the effect of pressure, iPP exhibits a "negative dependence" of crystallization kinetics upon pressure, with a decrease of density and degree of crystallinity with increasing pressure, owing to kinetic constraints. PA6 and PET, on the other hand, due to thermodynamic factors resulting in an increase in T_m with pressure, exhibits a "positive dependence" of crystallization kinetics upon pressure. Finally, recent original results concerning sPS have shown that the minimum in the density vs. cooling rate curve shifts toward larger cooling rates upon increasing pressure. Adv Polym Techn 28: 86–119, 2009; Published online in Wiley InterScience (www.interscience.wiley.com). DOI 10.1002/adv.20151

KEY WORDS: Cooling rate, Density, Morphology, Pressure, Processing

Introduction

Polymer transformation processes are based on a detailed knowledge of material behavior under extreme conditions that are very far from the usual conditions normally reported in the literature. In industrial processing, for instance, materials are subjected to high-pressure, high-shear (and/or elongational) rates, and high-thermal gradients. These conditions often lead to nonequilibrium conformational states, which turn out to be very difficult to describe using classical approaches. Moreover, it is easy to understand that the analysis of the relationships between processing conditions and the morphology developed is a crucial point for the characterization of plastic materials. If the material under investigation is a semicrystalline polymer, the analysis becomes still more complex by crystallization phenomena that need to be properly described and quantified. Furthermore, the lack of significant information regarding the influence of processing conditions on crystallization kinetics restricts the possibilities of modelling and simulating industrial material transformation processes, indicating that the development of a model, capable of describing polymer behavior under drastic solidification conditions, is very complex.

However, new innovative approaches can lead to a relevant answer to these scientific and technological tasks, as shown by some recent developments in polymer solidification analysis[1–3] under realistic processing conditions. These approaches are based on model experiments, emulating some processing conditions, and trying to identify and isolate the state variable governing the process.

So far, due to the experimental difficulties, the study of polymer structure development under processing conditions has been mainly performed using conventional techniques such as dilatometry[4–6] and differential scanning calorimetry (DSC).[7–9] Investigations made using these techniques normally involve experiments under isothermal conditions. However experiments under nonisothermal conditions have been limited to cooling rates several orders of magnitude lower than those experienced in industrial processes, which often lead to quite different structures and properties. Finally, in the past years, experiments revealing the crystallinity

evolution by measures of crossing light scattering, have been conducted at intermediate cooling rates.[10,11]

For the sake of completeness, it should be conceded that the complexity of the investigation concerning polymer solidification under processing conditions is even greater if the wide latitude of morphologies achievable is considered, especially when dealing with semicrystalline polymers. This would also have to take into account the complexity introduced by the presence of the crystallization process.[2]

Generally speaking, polymer crystallization under processing conditions cannot be considered an "equilibrium" phenomenon, since it is not possible to separate the thermodynamic effects on the processes from the kinetic ones. Furthermore, crystallization of polymeric materials is always limited by molecular mobility and very often leads to metastable phases, as recently shown by Strobl.[12] Further evidences of the formation of metastable phases under drastic conditions (high cooling rates and/or high deformation rates) have been widely reported for polypropylene (iPP)[13–15] for polyamide 6 (PA6),[16] and for poly(ethylene terephthalate) (PET).[17] Choi and White[15] described structure development of melt-spun iPP thin filaments, obtaining conditions under which different crystalline forms of iPP were obtained as a function of the cooling rate and spinline stresses. On the basis of their experimental results together with many others available in the literature, the authors have constructed a diagram that indicates the crystalline states formed at different cooling rates in isotropic quiescent conditions. Continuous cooling transformation curves have been reported on that diagram. According to the authors, at low cooling rates and high stresses, the monoclinic α-structure was formed, whereas at high cooling rates and low stresses a large pseudohexagonal/smectic ("mesophase") region was evident.

Recently, some evidence of the occurrence of a metastable phase when solidified from a quiescent melt has also been reported for PET.[18]

The formation of metastable phases normally takes place in a cooling rate range not achievable using the conventional techniques mentioned above; nevertheless, it is worth recalling that the behavior of a given semicrystalline polymer is greatly influenced by the relative amount of the constitutive phases. From this general background, the lack of literature data in this particular field of investigation should not be surprising, due to the complexity of the subject involved. The major task to tackle is, probably, to identify the rationale behind the multiform behavior observed in polymer solidification, with the aim of finding the basic functional relationships governing the whole phenomenon. Therefore, a possible approach, along this general framework, consists of designing and setting up model experiments that could help to isolate and study the influence of some experimental variables on the final properties of the polymer including its morphology. Thus a systematic investigation on polymer solidification under processing conditions should start with separate studies of the influence of flow, pressure, and temperature on crystallization kinetics.

Owing to experimental difficulties, there are only a few reports on the role of pressure in polymer crystallization, especially concerning its influence on the mechanical and physical properties. Moreover, the majority of studies made at high pressure have concentrated only on one polymer, polyethylene, dealing with the formation of extended chain crystals, as shown by Wunderlich and coworkers.[19–26] The pressure associated with such investigations tends to be extremely high (typically 500 MPa) with respect to the pressures normally used in industrial processes. Furthermore, the experimental conditions normally investigated were quasi-isothermal. This implies that the obtained results may not be applied to conventional polymer processing, involving very high thermal gradients.

The purpose of this work is to provide a general experimental route for studying the crystallization behavior of semicrystalline polymers under high cooling rates and pressure.

In this respect, two complementary devices were used. The first involves a special equipment that has been developed and widely tested, to quench polymeric samples at atmospheric pressure over a wide range of cooling rates (from 0.1 to ca. 2000°C/s) under quiescent conditions and with the use of which it has been possible to collect much information about the influence of the cooling rate on the final properties of the more widely used polymers, such as iPP, PET, PA6, and syndiotactic polystyrene (sPS).

The second was an innovative equipment specifically designed to evaluate the combined effect of typical injection molding pressures (up to 40 MPa) and temperature gradients (up to a maximum of ca. 100°C/s), with the aid of a modified injection molding machine. Data concerning iPP, PA6, PET, and sPS are reported.

The results show that the influence of pressure on polymer crystallization is not as obvious as one may expect. An increase of the cooling rate generally determines a transition from crystalline to noncrystalline (or pseudocrystalline) structures, not always accompanied by a monotonic density change, as shown by the example of sPS where the competition among α and β modifications, upon varying the cooling rate, gives rise to a minimum in the density vs. cooling rate curve. Furthermore, the effect of pressure fields superimposed on a given thermal history is strongly material dependent. In iPP, an increase in pressure results into a decrease of crystallinity, owing to kinetic factors (such as decreased mobility related to the increased T_g). In PA6 and PET, the opposite behavior is observed due to thermodynamic reasons (i.e., increase of T_m with pressure). In sPS, a shift in the minimum of the density vs. cooling rate curve takes place toward larger cooling rates, owing to the influence of pressure on the polymorphic behavior of the polymer.

Description of the Experimental Procedure

RAPID COOLING EXPERIMENT AT ATMOSPHERIC PRESSURE

A schematic drawing of the experimental setup is shown in Fig. 1a. The sample, properly enveloped in a thin aluminum foil, so as to avoid leakage of material while in the molten state (see Fig. 1b) and sandwiched between two identical flat metallic slabs, is heated to a suitable high temperature in a nitrogen-fluxed environment.

A fast response, 12.5-μm thick (omega-type CO_2), thermocouple buried inside one of the slabs allows recording of the whole thermal history by a data acquisition system.

A Cu–Be alloy was chosen for the production of the metallic slabs, owing to its high Young's modulus coupled with a high thermal conductivity (see Table I and *Goodellow Catalogue*[27]).

After keeping the sample system at a temperature above the equilibrium melting temperature for a time sufficient to erase memory effects,[28,29] the sample assembly was moved to the lower zone of the container where it was quenched by spraying a cooling fluid on both faces through two identical nozzles positioned symmetrically opposite each face of the sample assembly (Fig. 1a).

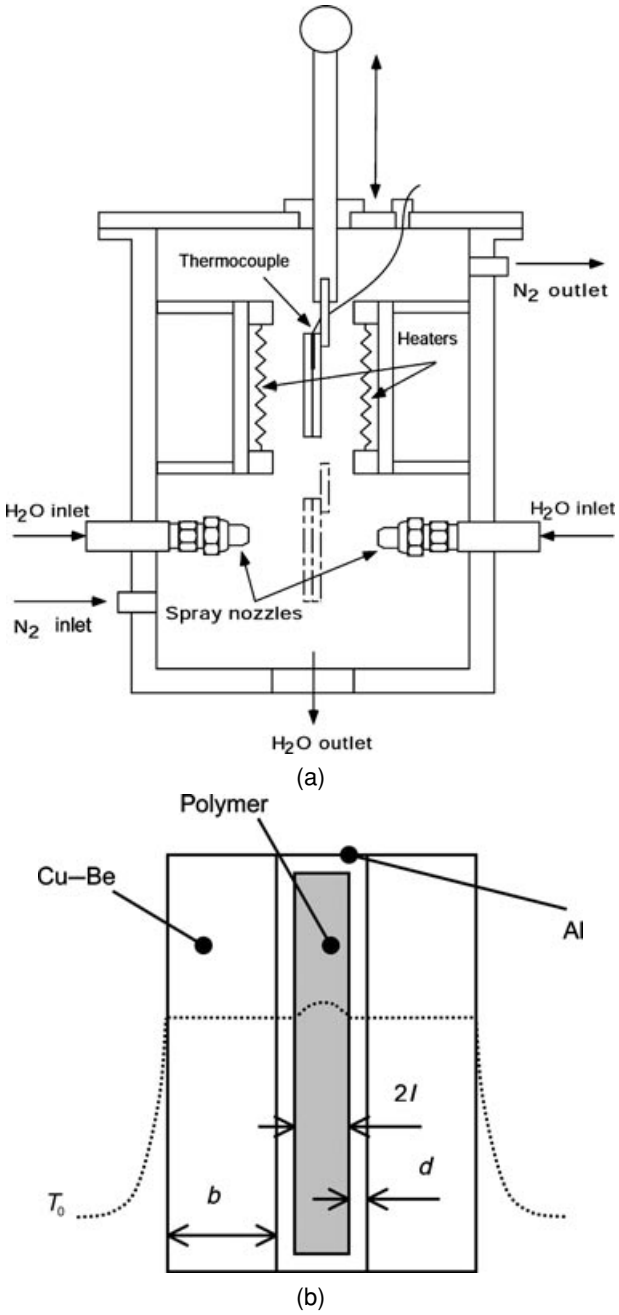

FIGURE 1. (a) Scheme of the experimental setup for quench experiments. (b) Sample assembly and temperature profiles. $b = 1$–2 mm; $l = 50$–100 μm; $d = 10$ μm. (From Brucato et al.[3]).

The cooling rate was varied by changing the cooling fluid, its flow rate, and temperature, or by changing the thickness of the sample assembly. However, the coolant temperature may not be crucial if it is sufficiently lower than the polymer solidification temperature.

TABLE I
Physical and Transport Properties

Material	ρ (kg m^{-3})	C_p (J Kg^{-1} K^{-1})	K (W m^{-1} K^{-1})	T_m (°C)
Cu–Be 2% alloy	8200	500	100	1000
i-PP	910	1926	0.15	170
PA-6	1150	1500	0.23	250
PET	1390	2300	0.147	280

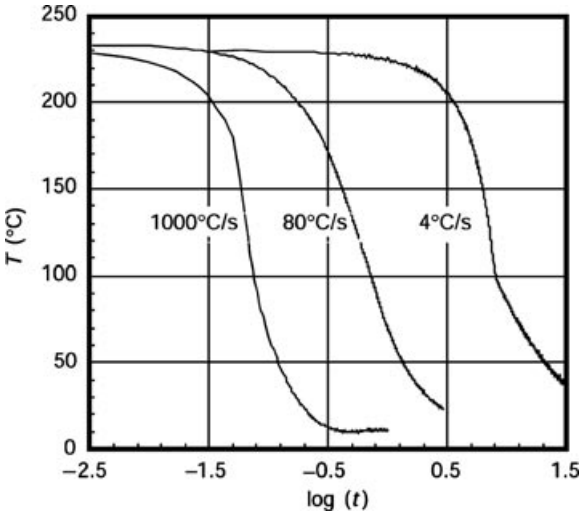

FIGURE 2. Typical thermal histories for spray-cooled samples (from Brucato et al.[3]).

Once the sample reached the final temperature, it was immediately removed from the sample assembly and kept at low temperature (−30°C) before further characterization. In the case of water sensitive polymers (PA6 and PET), the samples were preliminarily subjected to a drying procedure, according to the nature of the material.[18,30,31]

Three typical thermal histories (i.e., variation of temperature with time) obtained using this device are shown in Fig. 2. Results of an extended set of experiments are reported in Fig. 3 as recorded variation of cooling rate with sample temperature. The data in Fig. 3 represent the range of variation of cooling rate covering five orders of magnitude (0.01–1000°C/s). This result is particularly significant when compared to standard DTA or DSC runs which cover only the lowest two decades of this cooling rate range (0.01–1°C/s). It is worth noting that for crystallization kinetics the high cooling rates

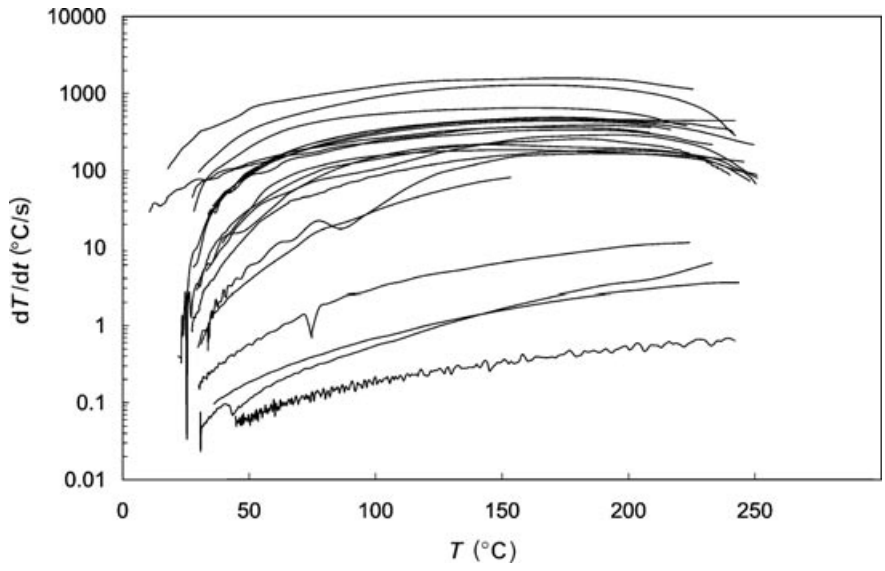

FIGURE 3. Typical experimental cooling rates variation with sample temperature (from Brucato et al.[3]).

are very informative, especially for fast crystallizing polymers, such as polyamides and polyolefins. However, the high cooling rates severely restrict the possibility of detecting the structural modifications taking place during solidification. The latter is the main constraint with respect to the real-time information provided by DTA and DSC measurements.

With respect to the thermal histories in Fig. 2, one will note that there is no temperature plateau associated with the crystallization process occurring during cooling. This is due to the fact that temperature was measured on the metal slabs and not in the bulk of the polymer sample, albeit the latter has a negligible mass and volume relative to the size of the metal slabs. Furthermore, the very high heat flux to which the polymer was subjected masks the effect of the latent heat of crystallization. So, only the temperature–time history is recorded and, therefore, at the end of the cooling process one gets a thin polymeric film with a known thermal history. Sample structure depends on thermal history, and this relationship can be experimentally assessed if the "length scale" of structural features developed is small compared to the sample thickness and if the final structural features are uniform throughout the whole sample.[32–34] The sample homogeneity is thus crucial to the method envisaged since the recorded thermal history is the only available information for the determination of the final structure of the sample.

The proposed model experiment is addressed to design a method for the characterization of non-isothermal solidification behavior, encompassing typical cooling conditions of polymer processing. Only temperature history determines the structure formed as melt solidification takes place in quiescent conditions.

A discussion on the temperature distribution in a monodimensional heat exchange regime and the experimental evaluation of structure distribution obtained along the thickness follows.

Cooling Mechanism

We will consider now the effect of the applied heat flux on the temperature distribution of the metal in the sample assembly. Later in the next section, the temperature distribution across the sample in contact with the metal will be examined.

The shape of the temperature profile in a flat slab having the following characteristics: thickness $2b$ and thermal conductivity k, and conditions, initial temperature T_i, suddenly exposed to a cooling medium at temperature T_0 and draining heat from the slab with a heat exchange coefficient h, is determined by the Biot number:

$$\text{Biot} = \frac{h \times b}{k} \tag{1}$$

For our experimental conditions, the highest value of the Biot number is estimated to be 0.3. Although this value does not fulfil the classical requirements for a flat temperature profile distribution within the slab (which requires Biot < 0.1), the slab "cooling time" is practically unaffected by slab conductivity; therefore, the so-called "regular regime" conditions still apply.[35] On the other hand, an estimate of the response time of the slab assembly can be easily taken as the time needed for the midplane to undergo 99% of a sudden drop of the wall temperature. The solution of such a transient heat conduction problem gives the characteristic time τ_R as[36,37]

$$\tau_R = \frac{2b^2}{\alpha} \tag{2}$$

where α and b are thermal diffusivity and half thickness of the slab, respectively. Using the values of $\alpha = 2.6 \times 10^{-5}$ m^2/s (copper–beryllium 2% alloy[27]) and $b = 0.001$ m in Eq. (2) (see Table I) gives $\tau_R = 0.07$ s. Note that the fastest cooling rate in our experiments has a characteristic time τ_A=0.33 s, which is about five times of τ_R. Furthermore, since the real wall boundary thermal condition on the slab is not as sharp as the assumed stepwise drop of the wall temperature, the heat conduction inside the assembly does not affect the cooling history to any appreciable extent. Applying a more realistic boundary condition, i.e. a wall temperature depending on the heat flux, does not lead to a sudden wall temperature drop, and the ratio τ_A/τ_R becomes larger.

In the experiments, water sprays were used to drain heat from the slab; therefore, the associated heat transfer coefficient depends very much on the flow rate of the cooling medium, as shown in Figs. 4a–4b. Here, the heat flux was evaluated according to the lumped temperature energy balance on a slab of volume $V = S \times 2b$, having a heat capacity c_p and density ρ:

$$\begin{aligned} \rho c_p V \frac{\mathrm{d}T}{\mathrm{d}t} &= h2S(T_0 - T) = -h2S(T - T_0) \\ \frac{\mathrm{d}T}{\mathrm{d}t} &= \frac{(T_0 - T)}{\tau_l} = -\frac{(T - T_0)}{\tau_l} \\ \tau_l &= \rho c_p \frac{b}{h} \end{aligned} \tag{3}$$

where S is the slab surface, h heat transfer coefficient, T_0 the coolant temperature, and T the lumped sample temperature. By assuming that the heat exchange coefficient h is constant, then the slope of the cooling rate vs. temperature curve is also constant, whereas the slab temperature decays exponentially with time.

Figure 4a shows that below the maximum and using smaller nozzles, giving lower mass flow rates, there are two heat transfer regimes separated by the Leidenfrost temperature, i.e. by the onset of temperature for the production of a boiling layer nucleated by the surface of the slab. In Fig. 4b, the increase of the coolant mass flow rate results in the disappearance of the Leidenfrost temperature and brings about an extension of the linear dependence of heat flux to a higher temperature range up to the maximum.[38]

As long as the heat flux depends on temperature linearly, a constant heat transfer coefficient can be

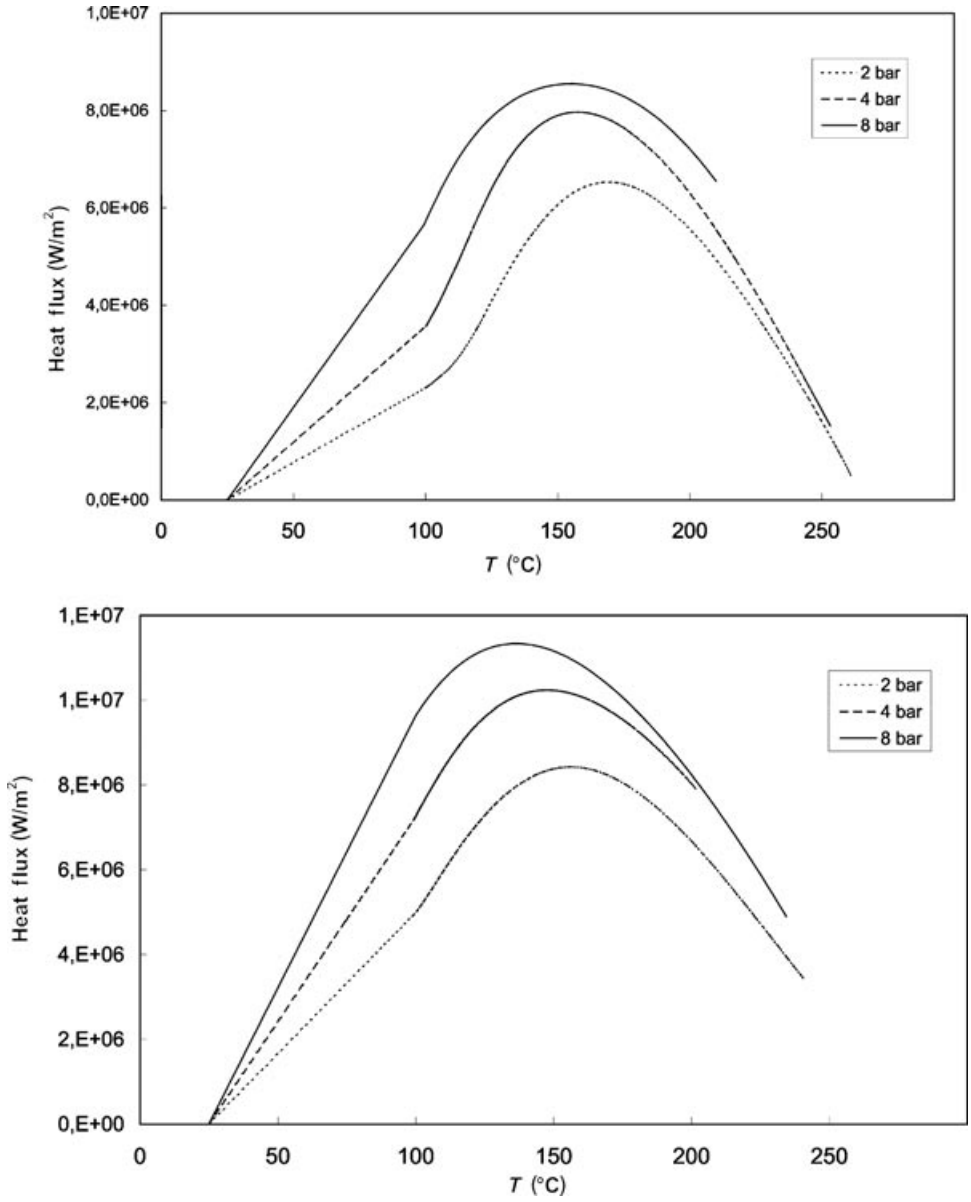

FIGURE 4. Heat Flux variation with sample assembly temperature for two different (a and b) spray nozzles (from Brucato et al.[3]).

successfully used. This condition is well satisfied in the low driving force (low-temperature difference) region.

This result can be understood considering that the heat transfer by convection induced by liquid drops impacting onto the solid surface is similar to that of nucleated boiling, because it promotes the renewal of the liquid layer close to the solid surface. Indeed, the two mechanisms take place in parallel and the spray cooling effectiveness can be varied by changing the mass flow rate of the coolant and, at high values of the mass flow rate, the same value of the heat exchange coefficient is attained in a temperature range spanning from ambient temperature to about 150°C. This last point is particularly relevant for fast-crystallizing polymers because high heat transfer coefficients are required at low temperatures to quench them effectively, as in the case of iPP and PA6.

The relationship between the liquid convection heat transfer coefficient, h, and the mass flow rate is summarized in Fig. 5 for all the nozzles used in this work. Within an error of ±10 there is a square root dependence of h on the mass flow rate.[38]

The time constant, τ_l, obtained from Eq. (3), attains a minimum value of about 0.05 s. A comparison of the values of $5 \times \tau_l$ and τ_R (98.5% of the overall temperature drop) shows that the driving force (i.e., the temperature drop) is larger in the fluid than in the Cu–Be slab, i.e. the heat transfer is mainly controlled by the fluid heat transfer. At the same time and the definition of τ_l suggests that another way to change linearly the slope of the cooling curves of Figs. 4a–4b is by modifying the slab thickness. Moreover Eqs. (2) and (3) show that the ratio τ_l/τ_R is proportional to the inverse of the thickness, suggesting that one should use the thinnest possible slab to achieve a more uniform temperature distribution through the thickness.

In principle, the time constant, τ_l drawn from Figs. 4a–4b could be used as a parameter to rigorously identify the overall cooling process.[1] When the solidification temperature of the polymer falls in a range in which there is a change of the heat transfer regime, the heat transfer coefficient will also change with temperature whereas the use of τ_l becomes meaningless, as it is no longer constant. On the other hand, the value of τ_l changes slightly when the temperature range, where solidification takes place, is quite narrow (of the order of 10°C). Although an average value of τ_l could be used, it is preferred to use an equivalent parameter to identify the cooling process, which is the average cooling rate in the range of temperatures within which the polymer solidifies.[3,13,14,18,30,39,40] This parameter, indeed, imposes not only the experimental time to be constant but also the characteristic range of temperatures in which a given polymer solidifies. For the polymers examined in this work (iPP, PA6, PET, and

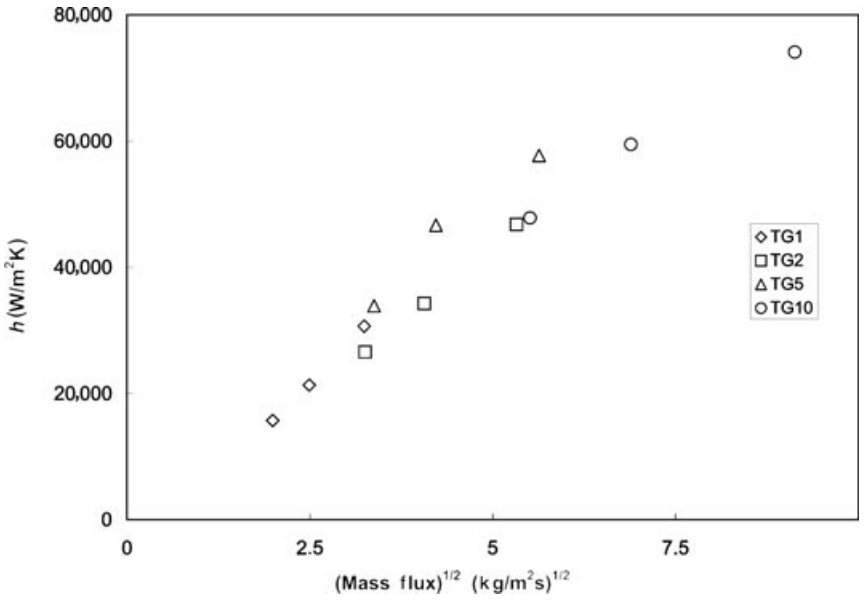

FIGURE 5. Dependence of heat exchange coefficient on coolant mass flux for four different spray nozzles (from Brucato et al.[3]).

sPS), the average cooling rates at around 70,[12,13,39,40] 135,[30,31,41,43] 170,[18,44] and 220°C[45] have been chosen as the parameters characterizing the cooling effectiveness for these polymers.

Although this is a semiquantitative measure of cooling effectiveness, the whole thermal history is available to compare experimental results with predictions from nonisothermal kinetic models.[14,18,30] Furthermore, if the kinetic constant vs. temperature relationship is mapped to the temperature vs. time profile, it is clear that an underestimate of the effective cooling rate is obtained only at low cooling rates. With an exponential temperature decay, most of the solidification takes place around the maximum of the kinetic constant, i.e. in the chosen temperature interval.

Temperature Distribution in the Polymer Sample

The solution of Eq. (3), introducing the dimensionless temperature of the copper–beryllium slab Θ_{Cu} with boundary conditions $T = T_i$ for t =0 and constant heat exchange coefficient, h, is

$$\Theta_{Cu} = \exp\left(-\frac{t}{\tau_l}\right) \tag{4}$$

where T_i and T_0 are the initial and final temperatures, respectively.

If sample thickness is very small compared to that of the slab, Eq. (4), representing the time dependence of the slab temperature (i.e., the temperature at the sample surface), becomes an exponential decay equation with a time constant defined by Eq. (3). Furthermore, in the case of very high cooling rates, this dependence of temperature on time extends to high temperatures. The smallest characteristic times are then obtained in the largest temperature range.

An estimate of the temperature profile in the polymer sample under these cooling conditions is, therefore, conservative and may well provide a case for achieving the maximum cooling rates with this technique, aiming to achieve a homogeneous thermal history throughout the entire sample thickness. As it has been previously pointed out, this condition must be satisfied to devise a direct relationship between the structures obtained and the associated thermal history.

The temperature distribution in the solid polymer sample can well be approximated by the Fourier equation for transient heat conduction within a medium of constant thermal diffusivity, i.e.

$$\frac{dT_{pol}}{dt} = \alpha \frac{\partial^2 T_{pol}}{\partial x^2} \tag{5a}$$

or in dimensionless form, i.e.

$$\frac{d\Theta_{pol}}{dFo} = \frac{\partial^2 \Theta_{pol}}{\partial \xi^2} \tag{5b}$$

where $\xi = x/l$ is dimensionless half depth; l slab half depth; Fo Fourier number, $Fo = \alpha t/l^2$; with the following boundary conditions:

(1) When $Fo = 0$ then $\Theta_{pol} = 0 \,\forall \xi$ (flat temperature profile before cooling);

(2) For $\xi = 0$, $\dfrac{\partial \Theta_{pol}}{\partial \xi} = 0 \,\forall\, Fo \geq 0$ (symmetry).

The cooled wall boundary condition is an exponential decay of temperature according to the following experimental observation:

(3) For $\xi = 1$,

$$\Theta_{pol} = \phi(Fo) = \exp\left(-\frac{t}{\tau}\right) \,\forall\, Fo \geq 0 \tag{6}$$

where τ is the exponential time constant (in s).

However, Eq. (5b) neglects the heat generated by the latent heat of crystallization. An analytic solution of Eq. (5b) with the boundary conditions given by Eq. (6) is provided in some texts,[46] i.e.

$$\theta_{pol}(\xi, Fo) = \frac{\cos(\xi \cdot \sqrt{Pd})}{\cos\sqrt{Pd}} \exp(-Pd \cdot Fo) + \sum_{n=0}^{\infty} \frac{2\cos[(2n+1)\pi/2 \cdot \xi]}{(\pi/2 + n\pi)\sin[(2n+1)\pi/2]} \exp\left(-\mu_n^2 \cdot Fo\right) \tag{7}$$

where $Pd = l^2/(\alpha \cdot \tau)$ is the Predvotitelev number (dimensionless time constant) and $\mu_n = \pi/2 + n\pi$.

The prediction of temperature profiles for an iPP slab (physical and transport properties presented in Table I,[47–49]) cooled with an exponential decay from $T_i = 230$°C to $T_0 = 5$°C is summarized for the case of two sample thicknesses (0.2 and 0.1 mm) in Figs. 6 and 7, respectively. The smallest time constant, $\tau_l = 0.05$ s, corresponding to the fastest experiment performed, is considered. Diagram (a) of

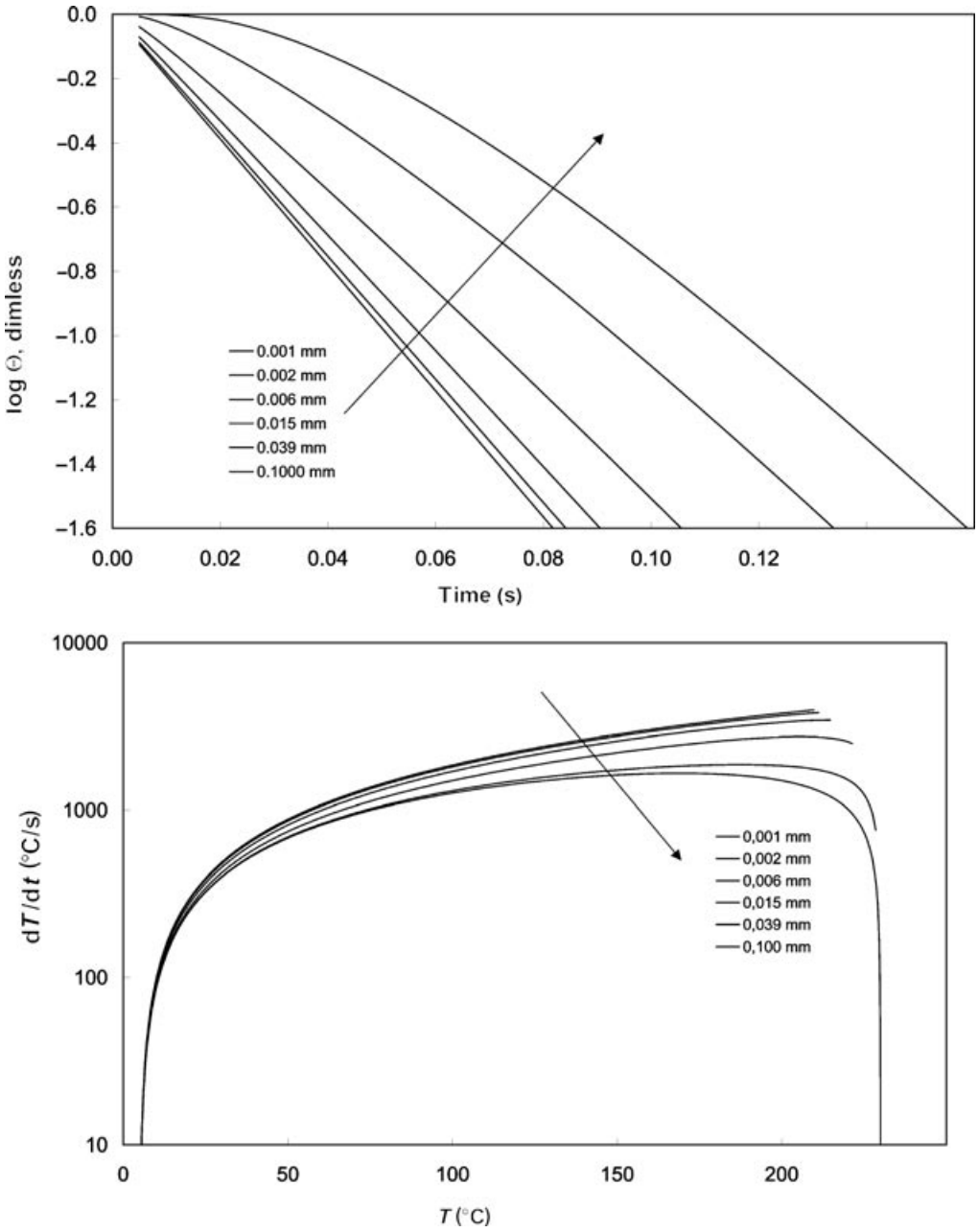

FIGURE 6. iPP film (half thickness = 100 μm) cooled from 230 to 5°C with an exponential decay with time for characteristic time $\tau_l = 0.05$ s. (a) Calculated temperature distribution across the thickness; (b) calculated cooling rate vs. temperature at different sample depths (from Brucato et al.[3]).

Figs. 6 and 7 shows the calculated temperature distribution across the thickness (only half sample is considered), whereas diagrams (b) shows the calculated dependence of the cooling rate on temperature at different sample depths along the thickness direction. One can observe that for a sample thickness of 0.1 mm (Fig. 7)], the temperature distribution is almost flat across the thickness. Significant deviations on the cooling rate vs. temperature dependence are observed only at temperatures significantly higher than the range of solidification for most polymers.

Although this result may appear to be in contradiction with the constraint expressed by Eq. (1), the analysis of the regimes involved in transient

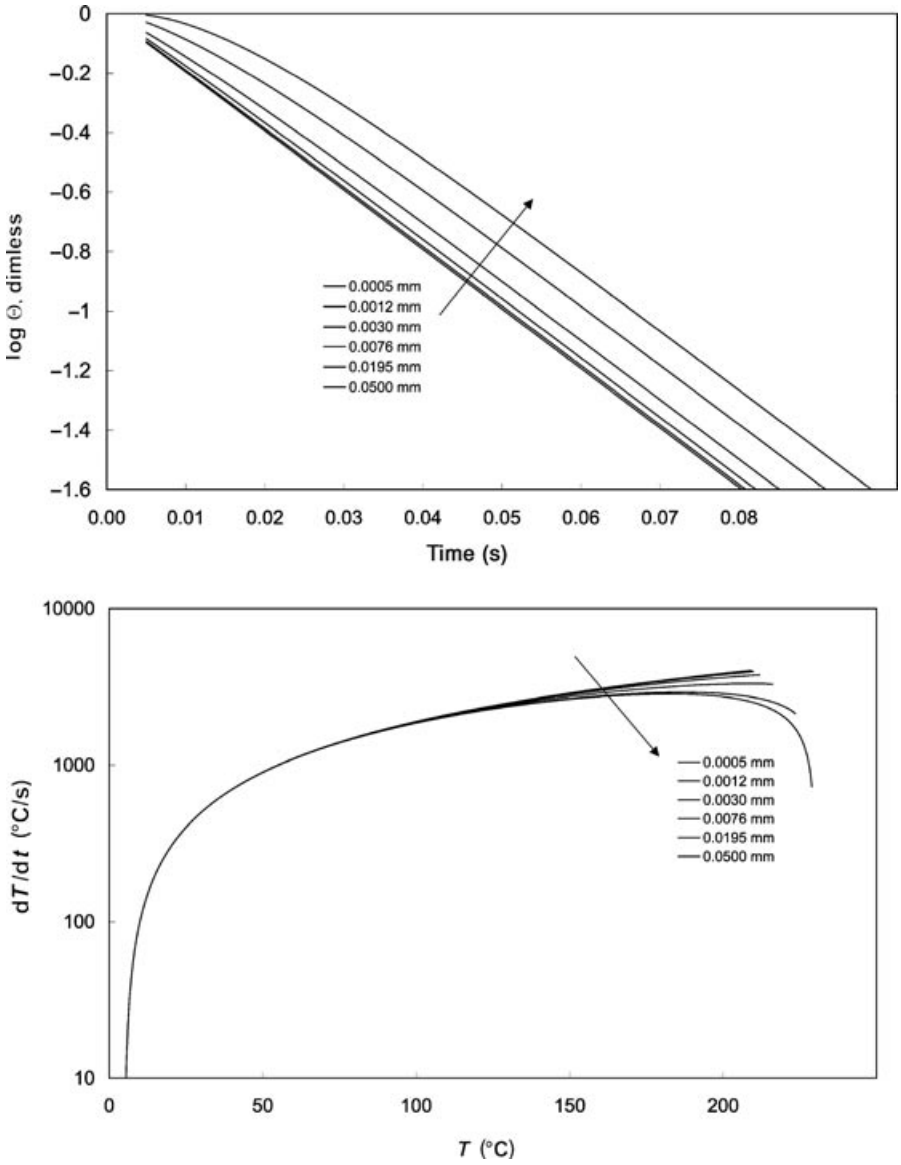

FIGURE 7. iPP film (half thickness = 50 μm) cooled from 230 to 5°C with an exponential decay with time for characteristic time $\tau_l = 0.05$ s. (a) Calculated temperature distribution across the thickness; (b) calculated cooling rate vs. temperature at different sample depths (from Brucato et al.[3]).

heat conduction, reported in advanced textbooks,[35] provides a consistent explanation. When a solid is suddenly exposed to a coolant kept at a constant temperature T_0, the temperature profile could experience two regimes: an initial one corresponding to dissimilar temperature profiles, and a second one, called "regular," whereby the temperature profiles are almost parallel to each other and self similar at different times. Depending on the Biot number, the second regime may also not take place and the condition Biot < 10 determines the onset of the second regime controlling the transient heat conduction for most of the cooling time. The condition expressed by Eq. (1) may thus be seen to be more restrictive than it is necessary, determining that the flat temperature is the controlling factor for most of the time during cooling of the solid from T_i to T_0.

In the regular regime of transient heat conduction, the onset of almost parallel temperature profiles determines a condition by which at different times the slope of the profile is the same in different sample positions, leading to the same cooling rate at the

same temperature and to a correct interpretation of the calculated results reported in Figs. 6 and 7. The temperature profile may thus be seen as a perturbation propagating from the external surface to the interior as the calculation in Figs. 6 and 7 shows.

For larger sample thickness, as in Fig. 6, although the temperature profile is not flat, the temperature distribution regime is regular and the cooling rate at lower temperatures is still almost constant throughout the sample. This is not so for cooling rates evaluated at temperatures higher than ca. 80°C. On the other hand, for small sample thickness, as is shown in Figs. 7, the heat transfer regime in the sample is always regular even at temperatures as high as 180°C.

As for the influence of the latent heat on the temperature distribution, which is neglected in Eq. (5b), one can observe that, although the heat of crystallization affects the temperature profile of the sample, and/or the thermal history to which it is subjected, the overall effect is only moderate. Indeed an estimate of the increase in sample temperature due to latent heat of crystallization, with the assumption that heat release takes place adiabatically, only produces maximum values of about 40°C, if the polymer sample crystallizes to the maximum allowable extent. Although this value may seem large when compared to the effect of temperature on the crystallization kinetics, it must be remembered that at low cooling rates, crystallization takes place over longer time intervals, and consequently does not affect appreciably the temperature of the sample because the heat is being released slowly. With respect to adiabatic conditions, a smaller temperature increase will, indeed, take place during cooling. Furthermore, the "heat sink" effect played by the metal slabs on the polymer film makes the temperature increase negligible. At high cooling rates, on the other hand, the heat is released in a shorter time interval; however, in this case, the temperature of the sample is controlled by very high heat fluxes and, consequently, the temperature is not affected very much either.[3,50,51] Moreover, if very drastic cooling conditions are applied, the sample only experiences a low degree of crystallization and, therefore, releases a smaller amount of heat, which affects the temperature even less.

RAPID COOLING UNDER PRESSURE

To evaluate the combined effect of typical injection molding pressures and temperatures, a new equipment was designed as a natural extension of the previously described apparatus. A standard Negri Bossi NB25 injection molding machine was used as a source of molten polymer supplied at a predeterminable and maintainable pressure at which the polymer can be injected into a preheated mold cavity.

A special injection mold has been designed such that samples could be cooled at a known cooling rate and under a known pressure.[3,51,52] This heated mold consists of a conical cavity (the sprue), which is located on the fixed platen of the injection molding machine, coupled to a "diaphragm." The front of the cavity is sealed with a high tensile, high thermal conductivity copper–beryllium "diaphragm," which is spray cooled on the opposite side when the quench starts. A schematic representation of the apparatus is shown in Fig. 8. The cavity is located within a brass block where eight cartridge heaters with a total power of 2 kW are inserted. The diaphragm is located in the moving platen of the machine. The whole apparatus (cavity and Cu–Be diaphragm) has been designed in such a way that it can be placed in and removed from an injection molding machine as a normal injection mold tool. A cooling channel, which allows the diaphragm to be spray cooled by pressurized water (at 8 bar) on one side, is also located in the mobile part. A thermocouple (type E, diam. = 0.05 mm) is inserted inside the diaphragm close to the wall facing the polymer sample to record the thermal history during cooling, while a pressure sensor (Dynisco PT46) mounted in the cavity allows measurement of pressure during the experiment. The pressure sensor and the thermocouple are connected to a data acquisition system, constituted by a National Instrument card LAB-LC coupled with an Apple-Macintosh LC computer.

The experimental methodology of recording the thermal history experienced by the surface of rapidly cooled samples and then analyzing the resulting sample morphology has been adopted. Using the above-described configuration, a thin layer in contact with the diaphragm solidifies under a known recorded thermal history and under a constantly recorded pressure history. Internal layers of the polymer are cooled with different cooling rates, which can be calculated by solving the transient heat transfer equation (7).[50,51] To relate thermal history to the structure formed, the relationship between the cooling rate evaluated at 70, 135, 170, and 200°C (characteristic temperatures of iPP, PA6, PET, and sPS, respectively,[3,13,14,18,30,39,42,45] and depth in the sample can be calculated based on the conduction heat transfer problem (Eq. (5)), as shown in Fig. 9. This is a sort of "transformation function" or "mapping function," which converts the depth in the sample in an equivalent value of the cooling rate, thus enabling

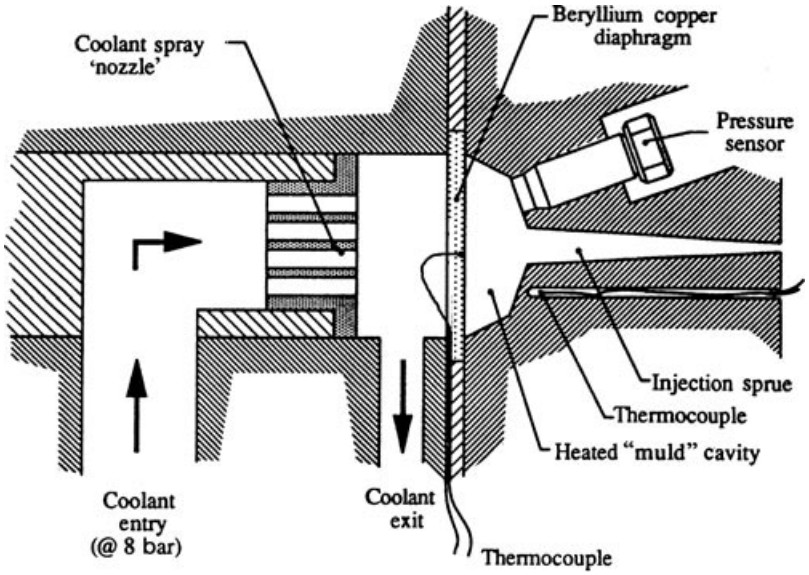

FIGURE 8. Scheme of the apparatus for solidification under pressure fitted to the modified injection molding machine (La Carrubba et al.[70]).

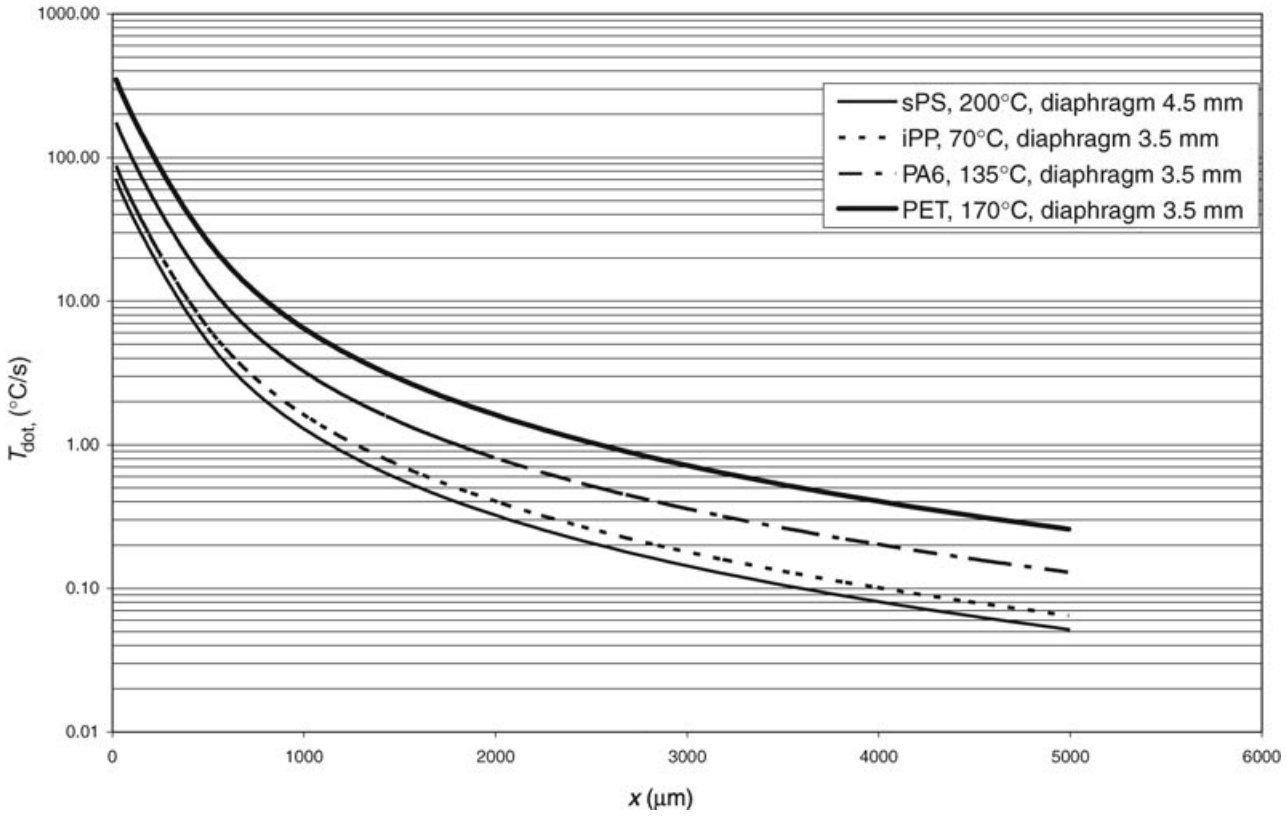

FIGURE 9. Depth–cooling rate "mapping functions" for iPP, PA6, PET, and sPS.

the physical data to be mapped as a function of the cooling rate rather than of the sample depth. This transformation functions allow the effect of pressure superimposed on that of the cooling rate to be properly identified and quantified.

Thin slices (50 μm) microtomed across a direction parallel to the cooled surface are then used for postsolidification characterization methods,[50–52] being each slice characterized by a well-defined cooling rate (averaged across slice thickness).

Materials and Characterization

The polymers studied were chosen with the aim of encompassing a wide range of crystallization behavior. It should be stressed, however, that while large differences in the crystallization kinetics exist between the different classes of polymers studied, the differences between material grades are generally of secondary order. The only exception is the effect of nucleating agents.[53]

The materials investigated include two polyamide 6 (PA6) grades, a polyethyleneterephthalate (PET), two polypropylene (iPP) grades (coded iPP3 and T30G), and a syndiotactic polystyrene (sPS). IPP3 and T30G (kindly supplied by Himont, Ferrara, Italy) have weight average M_w of 489,000 and 483,000, with a polydispersity index $I = 9.7$ and 6.4, respectively. PET (kindly supplied by Mossi & Ghisolfi, Tortona, Italy) has an intrinsic viscosity equal to 0.62 dL/g. As for PA6's, one grade (kindly supplied by Snia, Milano, Italy), was known to have $M_n = 18{,}000$ and $M_w = 38{,}000$. The other grade (kindly supplied by DSM, Heerlen, The Netherlands), only its average $M_w = 25{,}000$ is known. sPS with a weight-average molecular weight of 320,000 g/mol and a polydispersity index $M_w/M_n = 3.9$ was kindly supplied in pellet form by the DowChemical Co. (Midland, Michigan).

Thus a scale of sensitivity of the method proposed for describing the nonisothermal crystallization behavior could be assessed. The influence of a nucleating agent on the nonisothermal crystallization behavior at high cooling rates of the two PA6 resins has already been reported elsewhere.[42,54]

Since the cooling rate in the present devices is too fast for recording any macroscopic change during the solidification process, only the final structure of the solidified sample was evaluated. The final features of the samples, analyzed by suitable macroscopic probes, such as powder wide-angle x-ray diffraction (WAXD) patterns and density measurements were related to thermal history.

The x-ray diffraction measurements have been performed using a Philips vertical diffractometer equipped with a Philips PW1150 generator. The Cu Kα nickel-filtered radiation was detected at the interval 6°–45°, applying small steps of 0.05° in the range where crystalline peaks are present, and of larger steps of 0.2° elsewhere with a counting time of 60 s per step throughout.

The gradient column technique was used for density measurements. Details related to the choice of solvents have already been reported for iPP,[39] PET,[18,44] and sPS.[45] As far as the density measurements for PA6 are concerned, although the two liquids used in this work (*n*-heptane and carbon tetrachloride) are those almost universally used for PA6, the thin film samples did not achieve a stable position inside the gradient column, even by extending the observations to a few weeks. Obviously, the long residence time in the column can bring about density changes due to annealing of the sample and/or to sorption of the solvents used.

If the time scale in which sorption takes place is not superimposed on the time for the sample to fall to its equilibrium position, the sorption mechanism does not need to be known a priori. A correct analysis of the data, therefore, requires discriminating between the falling down toward the equilibrium position at the initial sample density and the change of position due to sorption. Falling motion of a body in a viscous medium having a linear density distribution has been described by Brucato et al. with the following expression:[31]

$$v = \frac{W}{k}\left[\left(1 - \frac{\rho_t}{\rho_s}\right) - \left(\frac{\mathrm{d}\rho}{\mathrm{d}y}\right)\frac{y}{\rho_s}\right] \tag{8}$$

where v is the falling velocity, W is sample weight, K is the ratio between drag force and velocity, ρ_s is sample density, and y is the depth from the level where the liquid density is ρ_t.

Equation (8) provides a linear relationship between the falling velocity v and the position y, since $\mathrm{d}\rho/\mathrm{d}y$ is a constant due to the linear dependence of density on the vertical coordinate normally fulfilled in gradient column techniques.

The falling behavior at short times is expected to be represented by a straight line in the v–y plane, if sorption is negligible. As the value of y at the equilibrium point (y_{eq}) is given by Eq. (8) when v is equal

to zero, a linear extrapolation of data to zero velocity leads to the determination of the "equilibrium density." Densities of samples cooled at constant cooling rate using a Perkin Elmer DSC7 were also measured.

Results

CRYSTALLIZATION OF SEMICRYSTALLINE POLYMERS AT ATMOSPHERIC PRESSURE

The data discussed in this section were obtained by quenching thin polymer films in the apparatus shown in Fig. 1. A comparison of the high cooling rate nonisothermal crystallization behavior of iPP, PA6, PET and sPS, showing very different crystallization behavior, is proposed with the aim to highlight any differences in the low cooling rate range and also in the range of cooling rates where the disappearance of the stable phase takes place. These examples will attempt to answer the question as to whether this method (which claims to assess the nonisothermal crystallization behavior from the structure-thermal history relationship only, without any local information on modifications taking place during the cooling process) is able to discriminate such differences in crystallization kinetics.

Isotactic Polypropylene

The results of the correlation for iPP3 between the structural features of quenched samples, assessed through the macroscopic probes (WAXD and density) and thermal history, identified by the relevant cooling rate in the range of temperatures where the polymer solidifies (ca. 70°C for iPP), are shown in Figs. 10 and 11 for density and WAXD patterns dependence on the cooling rate, respectively. Such results point out the features of the proposed method of characterization already reported by the authors,[13,39,42] with respect to change of structure and density with the cooling rate. A broad range of densities was identified as well as extreme structural features in the WAXD patterns. The WAXD patterns reported in Fig. 11 show that at low cooling rates only the stable α monoclinic phase is observed with small amounts of the β phase, as identified by the reflection at $2\theta = 16.1^{\circ}$. The crystalline order, determined by the width of the peaks, continuously decreases on increasing the cooling rate up to a point where only two broad diffraction peaks are observed, showing the presence of the so-called mesomorphic phase of iPP.[55] At intermediate cooling rates, the coexistence of the two phases is revealed, over a narrow range of cooling rates, by the superposition of the two broad peaks of the mesomorphic phase and the faint residues of the peaks related to the α monoclinic phase.

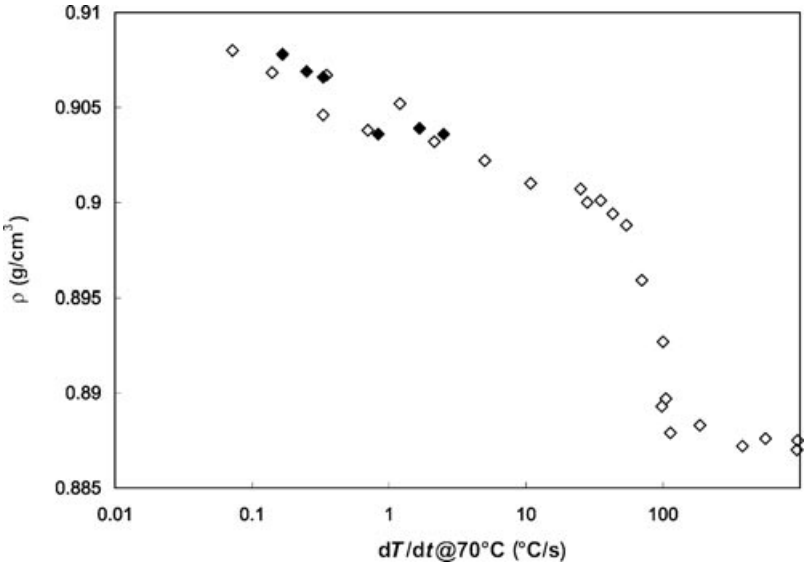

FIGURE 10. Density dependence on the cooling rate (measured at 70°C) of iPP3. (a) Open symbols: rapid cooling experiments; (b) filled symbols: standard constant cooling rate experiments (DSC; from Brucato et al.[3]).

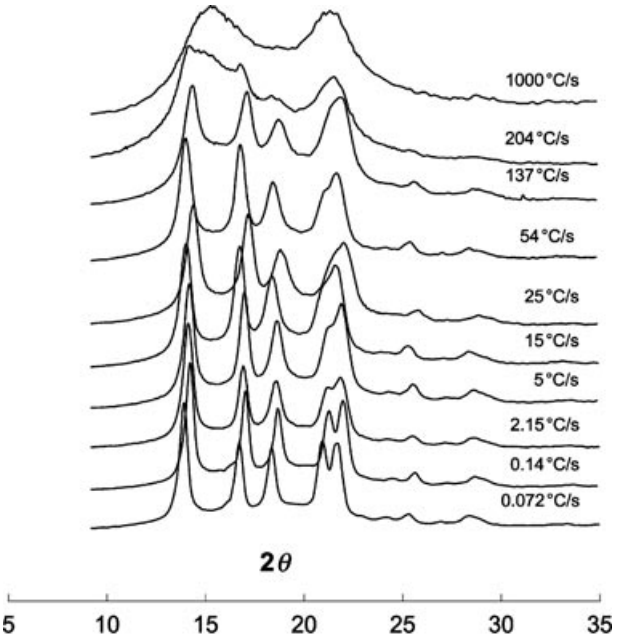

FIGURE 11. Dependence of WAXD powder patterns of iPP3 on the cooling rate (measured at 70°C; from Brucato et al.[3]).

Furthermore, changes in the WAXD patterns agree with the density measurements, making the two methods consistent and comparable. Although a qualitative cross-check can be made for the data in Fig. 11, a quantitative comparison can only be obtained by WAXD deconvolution.[56] This last technique has been extensively used to determine the phase content and its dependence on the cooling rate. This dependence of the phase content on the cooling rate, in turn, has been used for the determination of nonisothermal crystallization kinetics. The model adopted was based on the crystallization kinetics of two phases competing for the transformation from melt to solid.[31,39–42,52] The reason for two parallel crystallization mechanisms stems from the WAXD patterns dependence on the cooling rate. In the case of iPP, for example, the patterns show that the stable phase disappears while the mesomorphic phase content increases with increasing cooling rate. Similar behavior is shown for PA6, where the stable α–phase disappears and the γ and amorphous phases, respectively, form when we increase the cooling rate.

The density vs. cooling rate curve of Fig. 10 shows three zones characterized by different features related to the WAXD-based phase content dependence on the cooling rate reported in Fig. 12:

(i) At low cooling rates where only stable phases are formed, the density decreases to a small extent with the logarithm of the cooling rate.

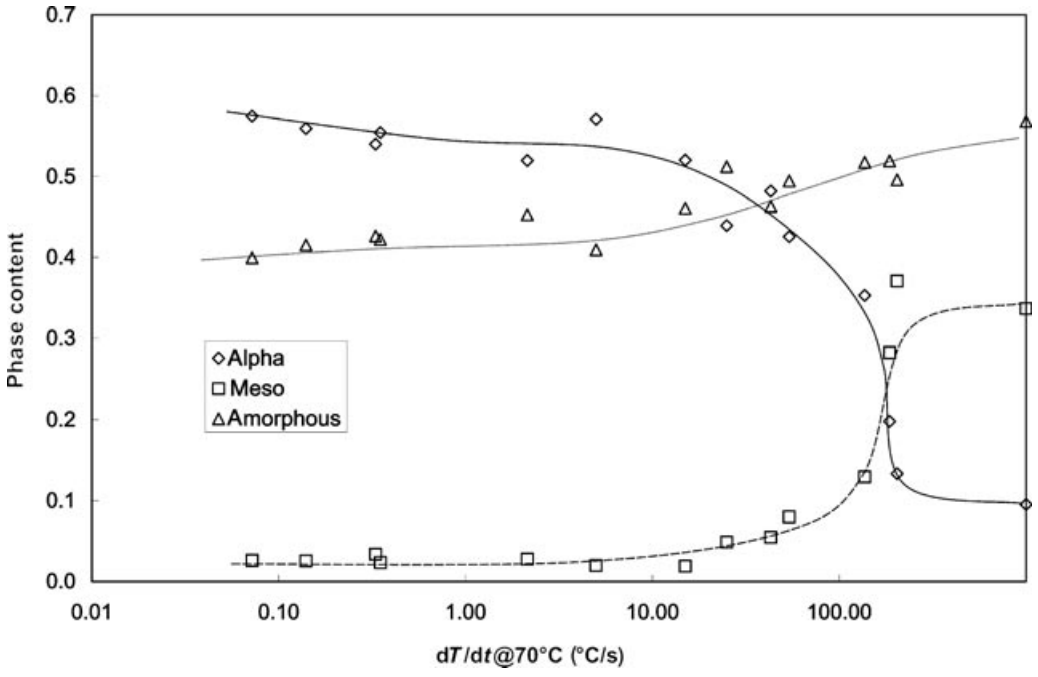

FIGURE 12. WAXD deconvolution of iPP3. Phase content vs. the cooling rate (measured at 70°C; from Brucato et al.[3]).

Below ca. 5°C/s, a slight decrease of density is observed, which is related to the formation of small amount of the β phase formed.[13]

(ii) At the highest cooling rates, a low-density plateau is observed related to the mesomorphic phase set in, because a limiting packing condition has been approached. The nature of the mesomorphic phase is not well known; the most acknowledged hypothesis being a packing very similar to the α-monoclinic phase but with a low range order.[55] The most significant feature of this phase, indeed, is that it transforms to the stable α-monoclinic phase on ageing, which is relevant to the postprocessing behavior of iPP. Previous studies point out that the kinetics of this transformation to be measurable only above 80°C.[57] More recent annealing experiments, discussed elsewhere[58,59], show that such transformation can take place at much lower temperatures and can cause significant density changes.

(iii) In an intermediate cooling rate range, the material density shows a very high sensitivity to changes in the cooling rate. In this zone, the stable phase content decreases, whereas that of the mesomorphic phase increases as the cooling rate increases. This transition is strongly dependent on the material characteristics, e.g., nucleating agents and molecular weight.[60] Solidification under these intermediate cooling rates shows the effect of the competition between the α monoclinic and the mesomorphic phases in the transformation from melt to solid. The slope of the density curve in this region is a measurement of the sensitivity of the crystallization kinetics toward the cooling rate for a given polymer.

To sum up, although the mapping of the structural features provides a general understanding of the relationship between the thermal history and the associated structure formed during a quenching experiment, the density dependence on the cooling rate provides an immediate, quantitative information on the nonisothermal crystallization behavior of the polymer. In this respect, the identification of the narrow range of cooling rates at which the transition from α monoclinic to the mesomorphic phase takes place provides quantitative information on the material nonisothermal crystallization kinetics.

A model-based interpretation of such transitional cooling rates performed on the crystallization kinetics parameters has been published recently.[31,43,53]

Polyethyleneterephthalate and Polyamide-6

The density dependence on the cooling rate for iPP (iPP3), PA6, and PET is reported in Fig. 13. This figure, although shows similar features of those already described in detail for iPP3, it reveals a quite different dependence of density with the cooling rate.

As expected, PET is the slowest crystallizing polymer with a sharp transition from the α triclinic to amorphous phase taking place in a narrow cooling rate range (between 1 and 3°C/s) where it shows an abrupt decrease of density.[18] After this transition, a plateau is reached at constant density of 1.337 g/cm^3. The slight density decrease above 3°C/s is related to the increase of the amorphous phase free volume content with increasing cooling rate. More recently, the presence of an intermediate phase relevant up to 100°C/s has been postulated. The glassy state, indeed, is approached at higher temperatures upon increasing cooling rates, and the resulting increased constraints on molecular mobility bring about a nonequilibrium configuration.

The data of Fig. 13 show results of both quench experiments and constant cooling rate DSC ramps. These results show that for each material there is a well-defined range of cooling rates where an overlapping of density results derived from both experiments. This clearly confirms the agreement between the two techniques. In the case of PET, it is worth noting that amorphous samples can also be obtained by DSC at the highest cooling rates available. This takes place because of the higher temperature range at which crystallization of PET occurs, coupled with the slow crystallization kinetics exhibited by this material. In such experiments, using liquid nitrogen as a cooling medium, the DSC used (Perkin Elmer DSC7) made it possible to reach a maximum constant cooling rate of ca. 200°C/min (3.3°C/s), losing control around 130°C. The WAXD patterns of Fig. 14, related to the PET examined, show that samples cooled at a constant cooling rate of 150°C/min, together with all the samples solidified at higher cooling rates, are fully amorphous. On the other hand, the samples cooled at 70°C/min show faint residues of the α triclinic phase whose presence can only be inferred by the deviation form the typical amorphous pattern observed and by the sample density, significantly

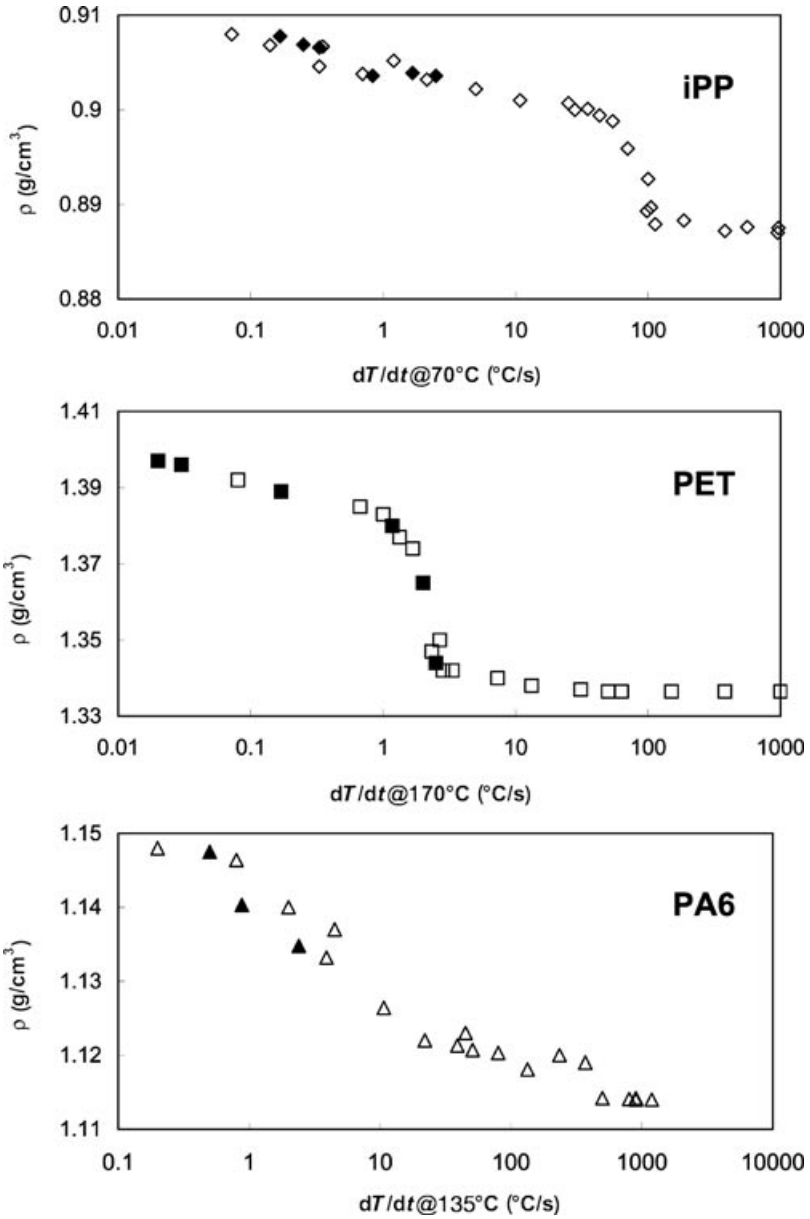

FIGURE 13. Density dependence on the cooling rate for iPP (iPP3), PA6, and PET. (a) Open symbols: rapid cooling experiments; (b) filled symbols: standard constant cooling rate experiments (DSC; from Brucato et al.[3]).

larger than 1.337 g/cm^3. This is a further typical example that the information provided by density and WAXD patterns agree and cooperatively provide insights into the structural features of the investigated sample.

Finally, PA6 shows an intermediate behavior characterized by a high-density plateau (stable α phase), a low-density plateau (γ phase, thermodynamically less stable), and a density drop occurring in the range 1–20°C/s. The PA6 density results shown in Fig. 13 also agree with the WAXD patterns reported in Fig. 15. This figure shows the residual α–phase peaks for the sample cooled at 22°C/s, whereas no more traces of the α–phase content are discernible in the patterns of samples cooled at higher cooling rates (Fig. 15).

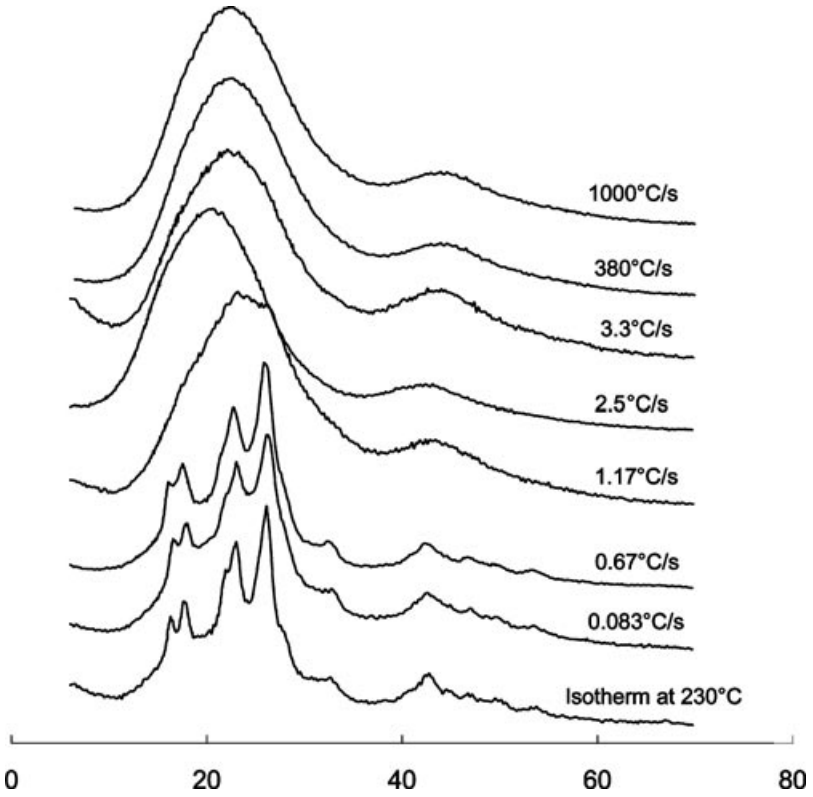

FIGURE 14. Dependence of WAXD powder patterns of PET on the cooling rate (measured at 170°C; from Brucato et al.[3]).

Syndiotactic Polystyrene

In Fig. 16, WAXD patterns are shown for quenched sPS samples in the angular range of 5°–19°, with an inset covering the entire range of 0°–45°. The crystalline peaks of the α phase are indicated by solid lines, and those of the β phase are indicated by dotted lines. Their positions are summarized in Table II.[61] A qualitative inspection of the patterns readily reveals the polymorphic behavior of sPS under rapid cooling conditions. In particular, one first observes that the material has the capacity to crystallize for cooling rates as high as 169°C/s, whereas for higher cooling rates (patterns of samples nominally quenched at 667 and 2600°C/s), the patterns do not show any reflections (even broader) and can be assumed to denote a completely amorphous material. However, one cannot exclude the possibility of some long-range structural order in the disordered state due to the nonequilibrium conditions of the amorphous state.[22]

Among the most crystalline samples, i.e. those obtained at lower cooling rates, three crystalline peaks

TABLE II
Syndiotactic Polystyrene Bragg distances (d_{obs}, Å) and Corresponding 2θ Positions of the α– and β–Phase X-Ray Reflections

					α Phase					
d_{obs}	13.11	13.07	7.58	7.51	6.56	4.94	6.31	5.67	4.37	4.34
2θ	6.7	6.8	11.7	11.8	13.5	18.0	14.0	15.6	20.3	20.5
					β Phase					
d_{obs}	14.37	8.48	7.18	6.52	4.78	4.39	4.18	2.56		
2θ	6.1	10.4	12.3	13.6	18.6	20.2	21.3	35.0		

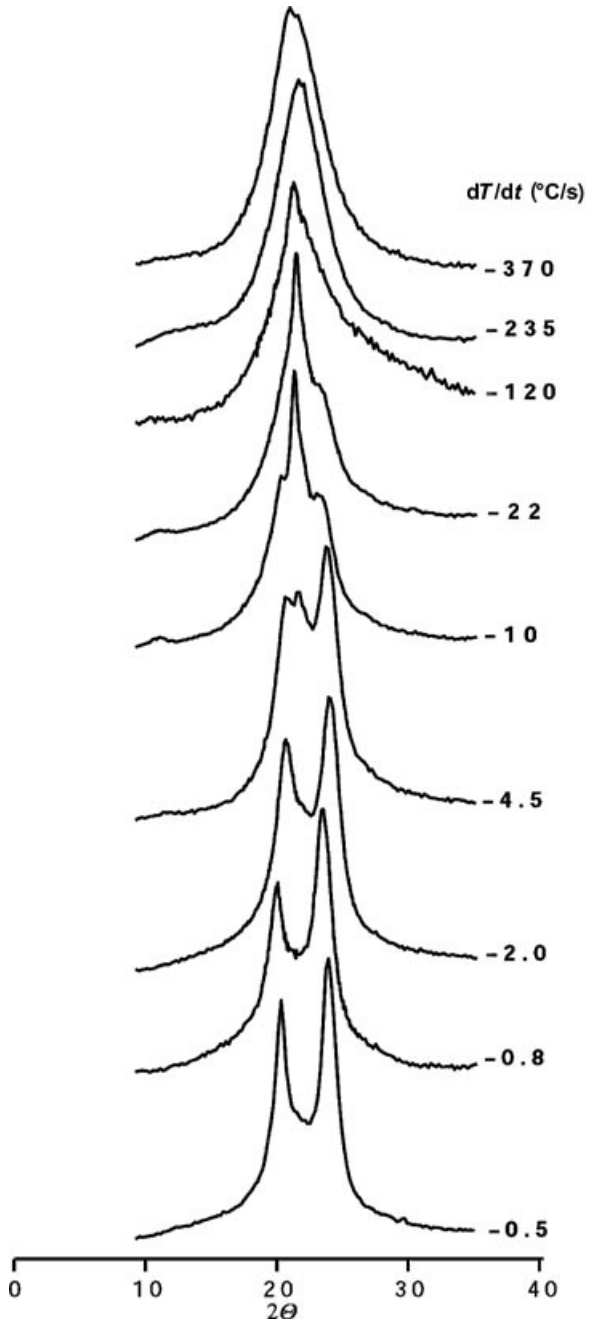

FIGURE 15. Dependence of WAXD powder patterns of PA6 (SNIA) on the cooling rate (measured at 135°C; from Brucato et al.[3]).

are clearly distinguishable, corresponding to 2θ angles of 6.76°, 11.67°, and 13.5°. The first peak (which is attributed to the α phase, see Table II) is not only the most intense but also the only peak exhibiting diffraction in the sample nominally quenched at 169°C/s. The two other intense peaks are also related to the α phase, remaining evident up to cooling rates as high as 17°C/s. Other α–phase peaks with lower intensities are located at 2θ angles of 15.6°, 17.95°, and 20.2° (see Table II).

When focusing on the most crystalline sample, i.e. the one solidified under the lowest cooling rate, 0.33°C/s, some more crystalline peaks are visible related to the β phase, positioned at 2θ values of 6.15°, 10.4°, and 13.2°. Although the same peaks are also discernible in higher cooling rate samples, the intensity of the last two peaks tends to reduce on increasing cooling rates, such that they turn out to be almost invisible for cooling rates greater than 2°C/s.

Finally, by looking at the patterns of the amorphous samples (for cooling rates higher than 169°C/s), only a halo clearly defined by two broad peaks located around 2θ values of 10° and 19.5°, respectively, can be observed.

To sum up, it is evident that all the peaks related to the α phase (the kinetically favored phase) are seen to persist up to relatively high cooling rates (ca. 20°C/s), whereas the peaks corresponding to the β crystalline modification (the thermodynamically favored one) tend to disappear at relatively low cooling rates (ca. 2°C/s).

These qualitative observations provide further confirmation of the results obtained from the deconvolution of the WAXD patterns, according to a procedure extensively reported elsewhere.[56]

In Fig. 17a, the overall crystalline ($\alpha + \beta$) and the amorphous fractions, obtained from the WAXD deconvolution as a function of cooling rate, are shown. A very high overall crystallinity, in the region of 70% is estimated for cooling rates lower than 1°C/s, which is a rarely observed with commercial polymers (excluding the case of polyethylene[19–25]), whereas at the maximum cooling rates only a few percent of residual crystallinity is attained. This is of the same order as the error involved in the WAXD deconvolution and can, therefore, be considered to be negligible. Although the crystallinity measured at low cooling rates in this paper appears to be unusually high, crystallinity values of the order of 60% in sPS isothermally crystallized from the glass at 150°C have already been reported by other authors.[62]

More interesting is the comparison of the phase content distribution of α and β phases, as shown in Fig. 17b where the β phase is observed, although in limited amount, only for low cooling rates (<1°C/s), becoming negligible at higher cooling rates. Hence, the α–phase content reflects the trend of total crystallinity (see Fig. 17) except for the first three cooling conditions (samples solidified at $dT/dt < 1$°C/s).

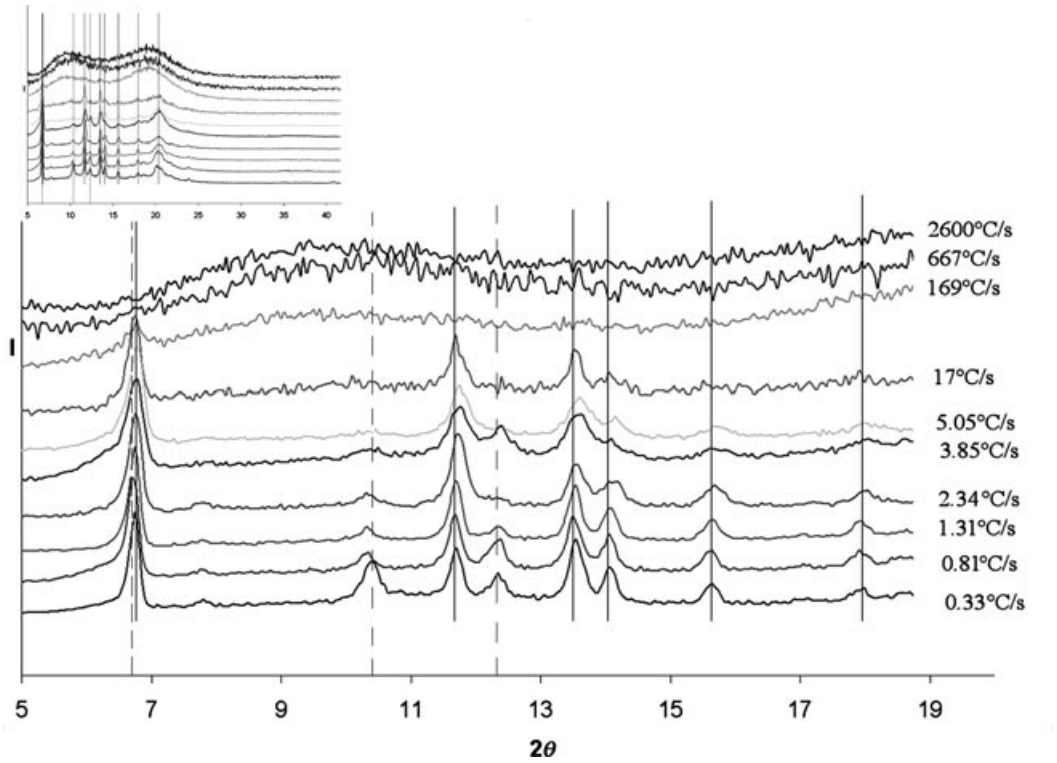

FIGURE 16. WAXD patterns of sPS samples quenched at different cooling rates (from La Carrubba et al.[45]).

The phase distribution provides a sound explanation for the density dependence on the cooling rate reported in Fig. 18. Moreover, it is also evident that the density dependence on the cooling rate goes through a minimum of around 1°C/s.

In the high cooling rate range, (dT/dt more than 500°C/s), there is a constant density plateau. This usually happens with all polymers, at very high cooling rates, favoring the formation of an amorphous phase or the onset of highly metastable low-range order pseudocrystalline phases, which have been identified for a large variety of polymeric materials, including sPS.[3,12,18,61,63,64] In the range between 1 and 500°C/s, a monotonic density increase is noted, which is in apparent contradiction with the behavior normally observed for semicrystalline polymers, where a decrease in the density with the cooling rate usually takes place.[65] It has to be borne in mind, however, that the anomalous density value of the amorphous phase (larger than the one of the α phase), is responsible for the observed increase in density with increasing cooling rate. Finally, in the low cooling rate range, between 0.3 and 1°C/s, there is a continuous monotonic density decrease, followed by a density minimum for a cooling rate of ca. 1°C/s.

To understand this behavior, one must remember that at low cooling rates the thermodynamically most stable phase is the β phase, whereas at larger cooling rates only the kinetically favored α phase is detected. Hence, the observed density minimum results from a competition between the thermodynamically stable β phase (the most dense phase) forming at low cooling rates and the kinetically favored α phase (the least dense) forming at moderate cooling rates.

On the basis of this experimental evidence, the minimum in the density data presented in Fig. 18 can be easily explained by the following reasoning. The overall density may be calculated from the following expression:

$$\frac{1}{\rho} = \frac{X_\alpha}{\rho_a} + \frac{X_\beta}{\rho_\beta} + \frac{X_{\text{am}}}{\rho_{\text{am}}} \tag{9}$$

where phase densities values for ρ_α, ρ_β, and ρ_{am} can be obtained from the literature[61] and phase fractions (X_α, X_β, and X_{am}) are derived from WAXD deconvolution (Fig. 17b).

In Fig. 18b, a comparison between density calculated through Eq. (1) and experimental data (shown in Fig. 18a) is shown. From this comparison, it is

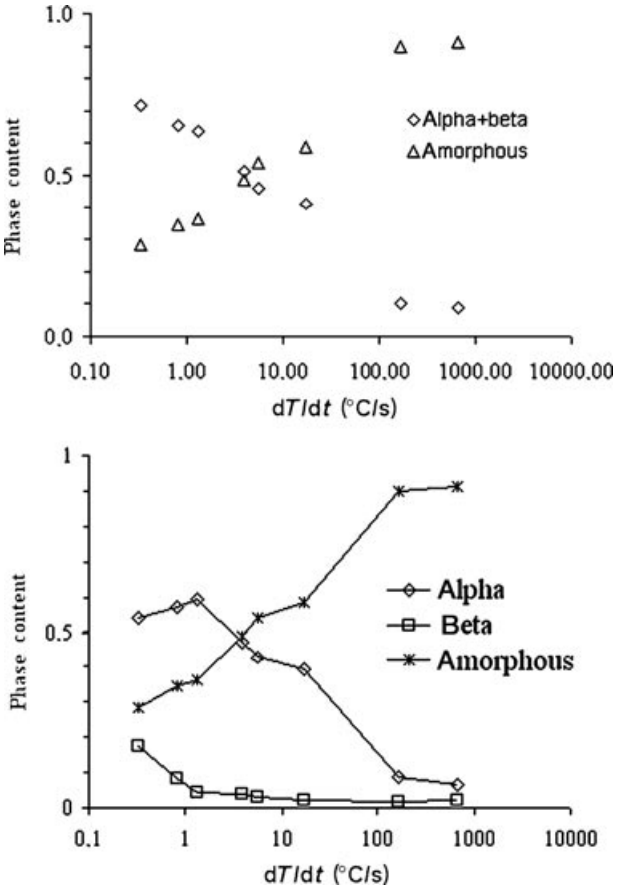

FIGURE 17. (a) sPS overall crystalline ($\alpha + \beta$) and amorphous fractions as a function of cooling rate. (b) sPS phase content as a function of the cooling rate (from La Carrubba et al.[45]).

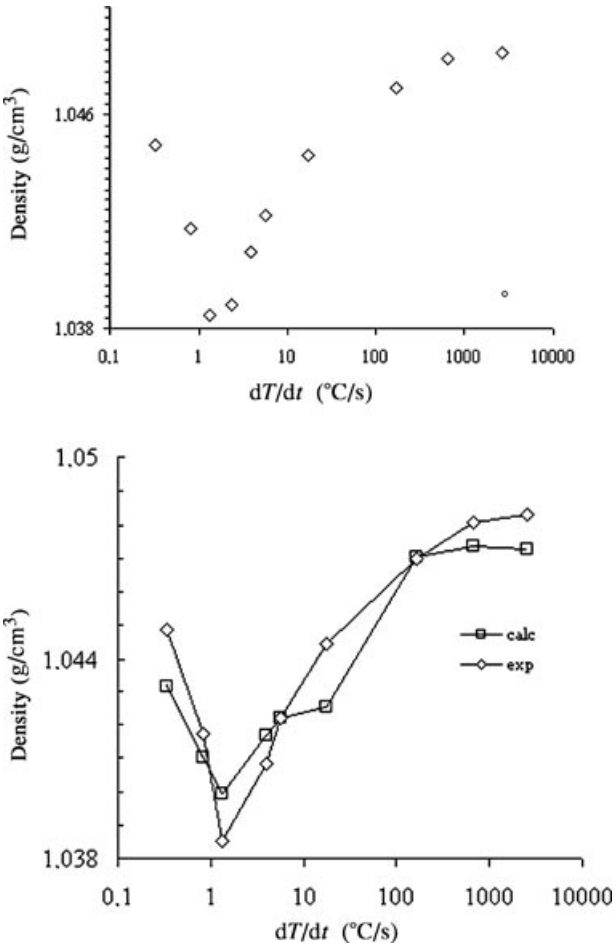

FIGURE 18. (a) sPS density as a function of cooling rate; (b) sPS experimental and calculated density data (from La Carrubba et al.[45]).

clear that it is possible to accurately predict the occurrence of a density minimum at a cooling rate of around 1°C/s.

It is the peculiar structure of the α phase[66] that is responsible for this behavior having a density less than the amorphous structure, which can give rise to clathrates as opposed to the β phase. The peculiar density relationship of sPS is similar to a few other polymers, for example, isotactic poly-4-methylpentene 1, iP4MP1, where amorphization by a pressure increase may be reversibly induced.[67,68] This behavior has been interpreted through a detailed phase diagram in a recent paper.[69]

CRYSTALLIZATION OF SEMICRYSTALLINE POLYMERS UNDER PRESSURE

In the following paragraphs, the nonisothermal crystallization behavior under pressure of iPP, PA6, PET, and sPS is examined to assess the sensitivity of the crystallization kinetics to pressure. A different density (and crystallinity) dependence upon pressure is observed for iPP on the one hand, and PA6 (and PET) on the other hand. The former exhibits a density decrease with pressure, and the latter shows a density increase with pressure. Finally, sPS data will be presented as an example showing the influence of pressure on the complex polymorphic behavior exhibited by this material, where the presence of a pressure field shifts the α to β transition toward larger cooling rates.

Isotactic Polypropylene

The results of the density measurements made on iPP T30G samples solidified under pressure are

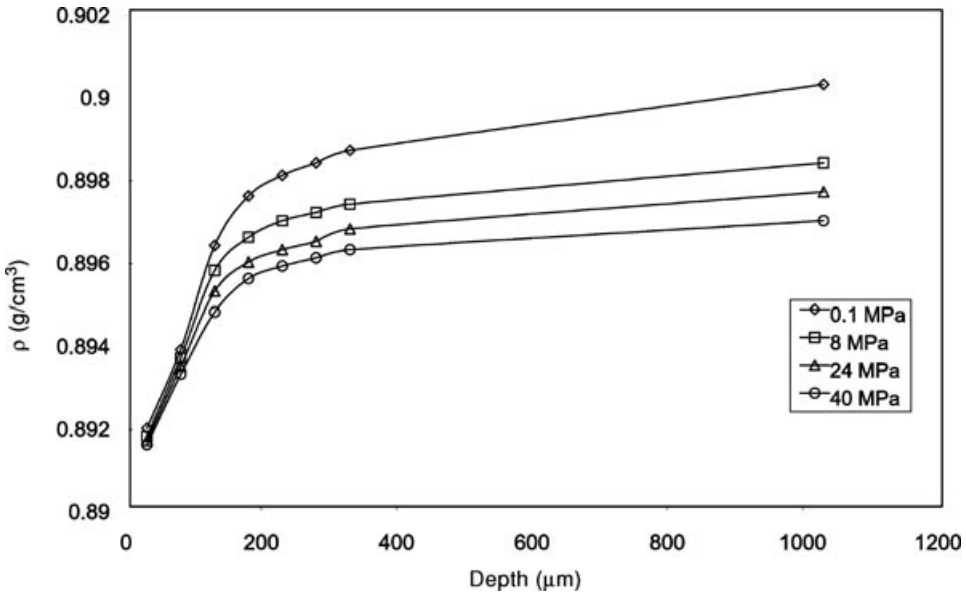

FIGURE 19. iPP (T30G) density depth profile (diaphragm 3.5-mm thick) for different solidification pressures from 0.1 to 40 Mpa (from La Carrubba et al.[52]).

reported in Figs. 19 and 20. Four different pressure conditions have been explored: 0.1, 8, 24, and 40 MPa using two different diaphragm sizes 3.5 and 8 mm thickness (see Fig. 8). In Fig. 19, the density depth profile for the 3.5-mm thick diaphragm is shown, and in Fig. 20 the density depth profile for the 8-mm thick diaphragm is shown. Samples obtained with the 3.5-mm thick diaphragm were subjected to an experimental surface cooling rate (measured at 70°C)[13,50,70] of about 100°C/s. Samples solidified using the 8-mm thick diaphragm experienced a surface cooling rate of about 20°C/s. It is worth noting that the surface cooling rate depends on the coolant heat transfer and on the diaphragm thermal

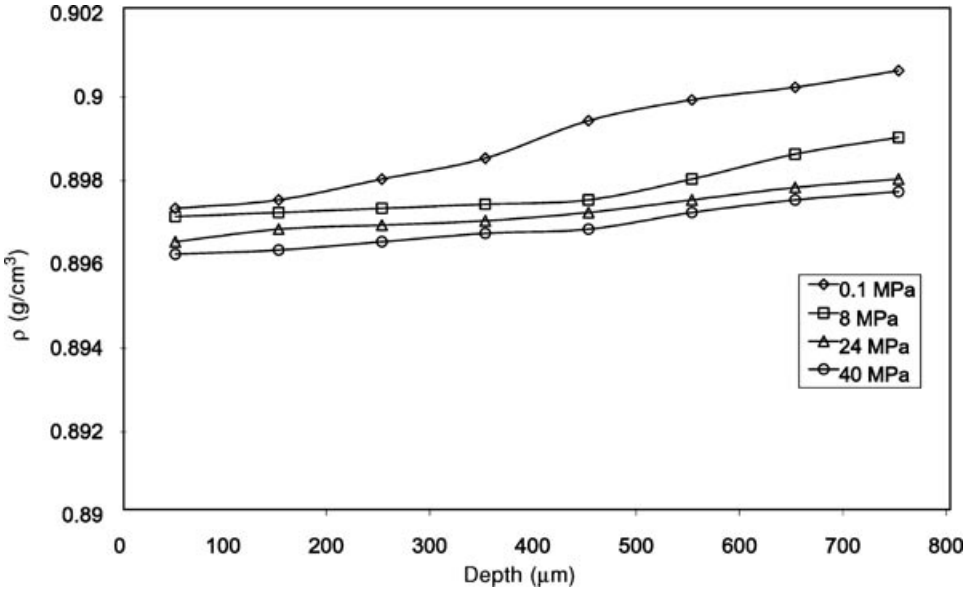

FIGURE 20. iPP (T30G) density depth profile (diaphragm 8-mm thick) for different pressures from 0.1 to 40 Mpa (from La Carrubba et al.[52]).

inertia. Changing the diaphragm thickness is, indeed a simple and reliable way to tune the surface cooling rate.[51]

The curves in Figs. 19 and 20 show that, for both experiments and at all pressures, density increases from the surface to the bulk of the sample. This behavior can be related to the expected increase in crystallinity because the internal layers are cooled at progressively lower rates. In Figs. 19 and 20, it is shown that the highest level of the density increase takes place in the vicinity of the surface and that this is independent of the applied pressure.

Both Figs. 19 and 20 also show somewhat unexpected results, in so far as a density decrease with pressure occurs at all depths in the sample. The reduction in density due to pressure is minimum at the sample surface and grows with the depth. Furthermore, the majority of the density change is observed by varying the pressure from 0.1 to 8 MPa, which is quite low especially if compared with the typical pressure values used in injection molding. This experimental result may be relevant for modeling the shrinkage and the internal stress distribution in injection-molded products. Particularly important is the fact that this effect is more pronounced in the bulk of the sample.[32–34]

Figure 21 is obtained by plotting the density data in Figs. 19 and 20 against the cooling rate calculated at 70°C by using a transient heat conduction model (Eq. (5); see La Carrubba et al.[70]). The value of the calculated cooling rate was averaged across every slice (50 μm thick). The use of the transient model was also validated by overlapping the data referred to a surface cooling rate of 100 and 20°C/s. In Fig. 21, it is also shown that at the constant cooling rate the final density decreases with pressure. The same trend is obtained with respect to the cooling rate, indicating that the density drop above 10–20°C/s is independent of the solidification pressure. Finally, Fig. 21 shows that the decrease of density with pressure vanishes with increasing cooling rate, implying that the influence of pressure is more pronounced in the bulk of the sample. This is a very important information in process simulation.

A similar pressure dependence of the density has also been observed by He and Zoller[6] using a standard dilatometer and measuring the specific volume of this sample during crystallization from the melt. A constant slow cooling rate (2.5°C/min) under constant pressure was used, bringing the sample back to a fixed pressure at the end of the test. It is worth noting that the majority of experiments have provided information on specific volume under pressure, whereas in our work we have measured the density at ambient pressure after solidification under pressure. He and Zoller observed an increase of

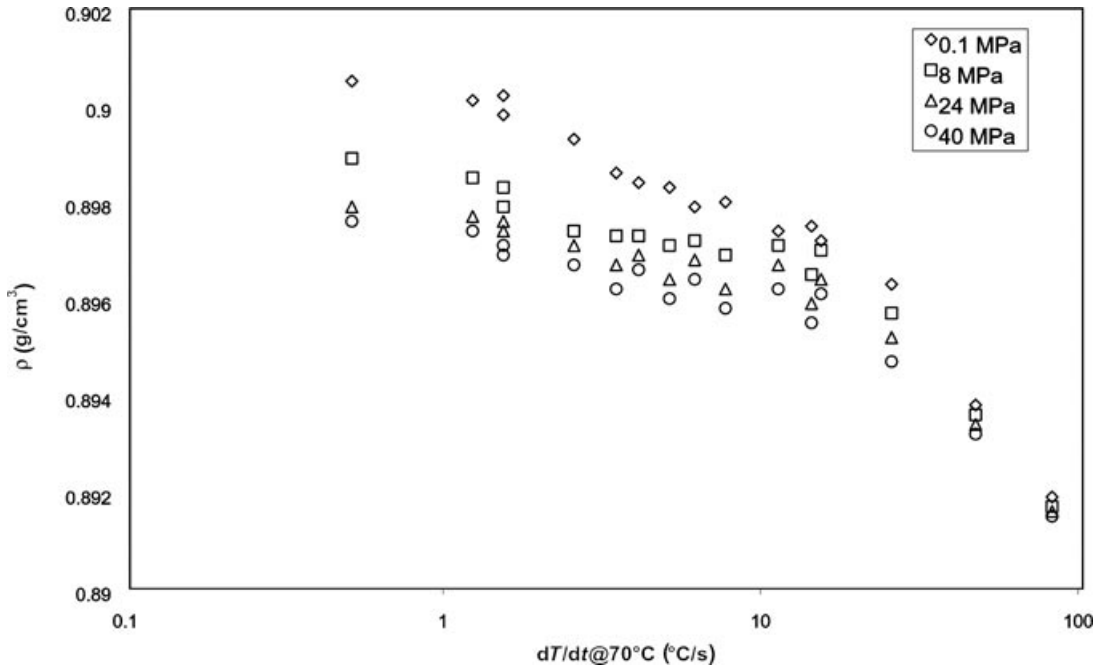

FIGURE 21. iPP (T30G) density vs. the cooling rate evaluated at 70°C for different solidification pressures from 0.1 to 40 Mpa (from La Carrubba et al.[52]).

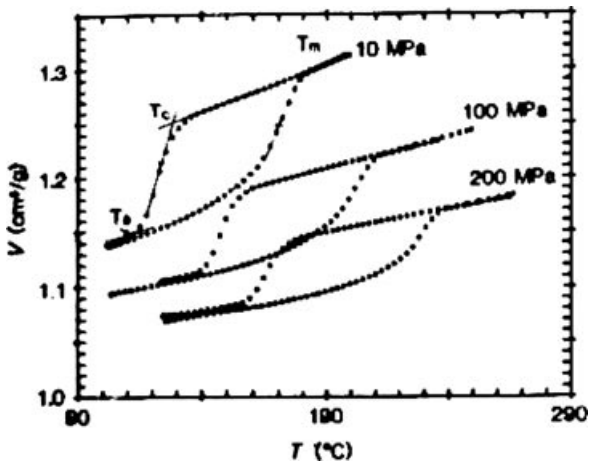

FIGURE 22. PVT curves of iPP (reproduced from He and Zoller[6]).

specific volume with increasing crystallization pressure in the case of iPP, whereas PA66 and PET have shown the opposite behavior.[6] In Fig. 22, the isobaric curves for iPP, at 10, 100, and 200 MPa from the same article,[6] related to melting and solidification, are shown. It is noted that, in all cases, the specific volume in the solid phase at the end of the solidification curve is slightly higher than the one measured at the beginning of the melting curve. This behavior demonstrates that during solidification under pressure some structural transformations take place giving final lower density values. Although He and Zoller have attempted to explain the reduction in the density with the formation of the γ phase, which is less dense than the α phase, the samples in our study did not show any evidence in the presence of the γ phase.[70] The last part of the solidification isobars in the low-temperature region in Fig. 22 shows the specific volume of the solid while it is held at the measurement pressure (i.e., 10, 100, and 200 MPa). When pressure is released, the volume expansion results in a higher specific volume. In the case of the experiments performed by He and Zoller, the final specific volume after expansion from 100 to 10 MPa turned out to be higher (i.e., lower density) than the specific volume measured at 10 MPa. This is in agreement with our results, which show that the final density (measured at atmospheric pressure) of samples solidified under pressure is, in fact, lower than that of the samples solidified at atmospheric pressure. We have repeated the PVT measurements on iPP and have published the results in a recent paper,[71] where a comparison between specific volumes of samples crystallized at different pressures and/or cooling rates has revealed a decrease in density with increasing cooling rate and pressure.

Thereafter, WAXD experiments were performed on slices cut in the transverse direction with respect to the direction of the heat flux. All experiments were performed by the synchrotron radiation source of the DESY center in Hamburg, Germany. A very long accumulation time (five frames of 1 min) was applied to achieve statistically significant results and a good reproducibility.

A qualitative analysis of the diffraction patterns has led to the conclusion that the α-phase content decreases on increasing cooling rate, for all the adopted pressures used.[50,52,70] The data have shown that an increase in pressure decreases the α-phase content. This is better shown by the WAXD data after a deconvolution procedure that has already been discussed elsewhere.[59] The program employed (implemented on MATLAB) uses a best-fitting procedure to calculate the positions and the intensity and of the α-phase including mesomorphic phase peaks and that of the amorphous halo.[59]

In Fig. 23, plots of the phase content of the samples against pressure at four different values of cooling rates, ranging from 1.5 to 80°C/s, are shown. A decrease in the α-phase is noticed, which is in agreement with the data from density and microhardness measurements, showing that the change in the α-phase content with pressure is the highest within the first 10 MPa. By examining the data in Fig. 23, one can note that the decrease in the α-phase with pressure tends to vanish when the cooling rate increases, particularly for cooling rates above 20°C/s. In addition, the reduction in the α-phase is mostly balanced by an increase in the mesomorphic phase content whereas the amorphous phase seems to be only slightly affected by pressure.

This last point is also very relevant, insofar as it shows that as the main effect of pressure is to replace the α phase by the mesomorphic phase, leaving almost unaffected the amorphous content. It has been already shown, in fact, that the main effect of increasing the cooling rate at ambient pressure is the substitution of the α phase with the mesomorphic one.[13,52] In other words, the qualitative effect of pressure (at a constant cooling rate) on the final structure appears to be the same as an increase in the cooling rate alone at a constant pressure.[70] This results is also illustrated in Fig. 24, showing the phase fraction, as calculated from the WAXD deconvolution of the samples, crystallized at atmospheric pressure using the rapid quenching apparatus. One can easily

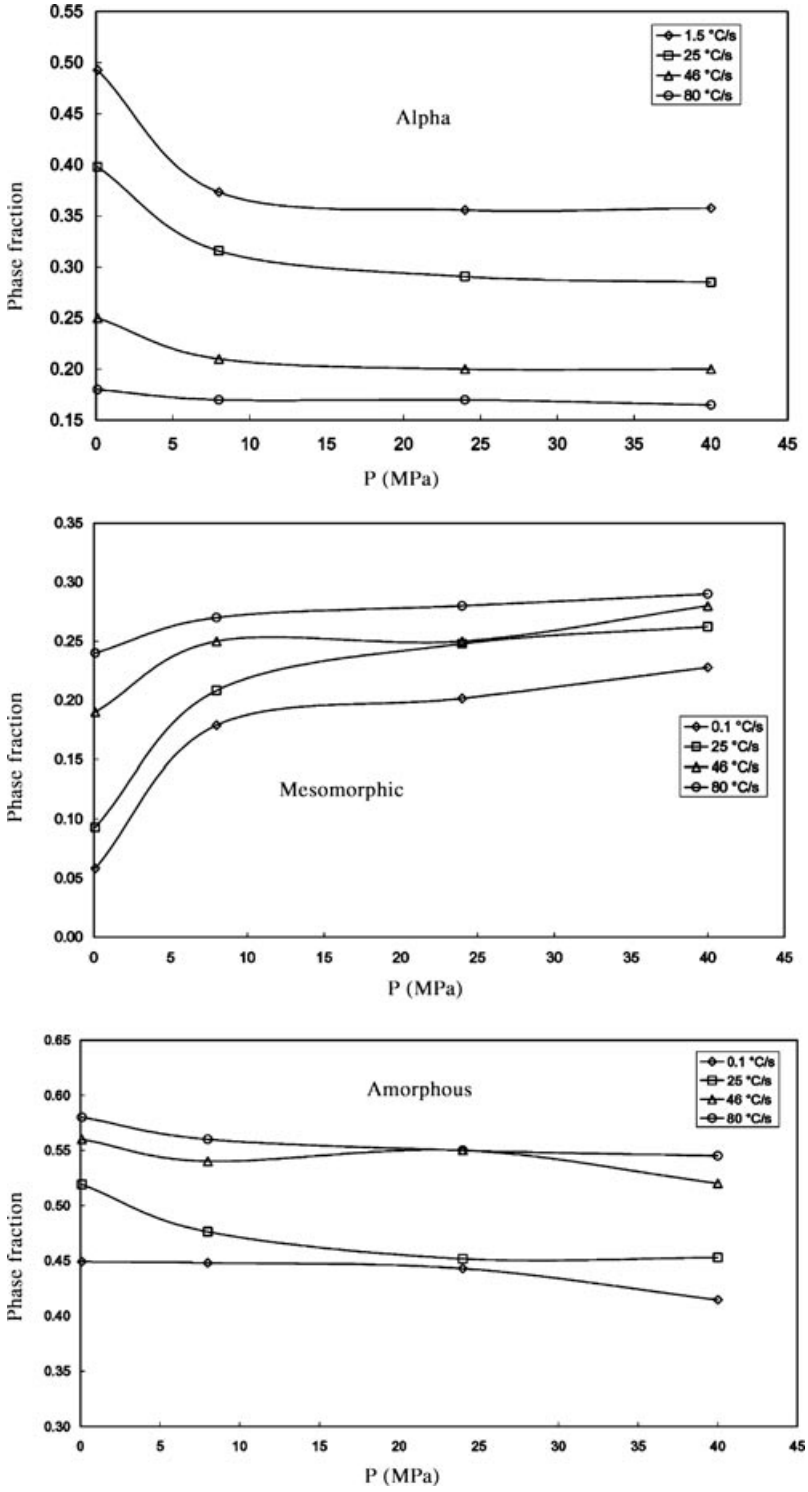

FIGURE 23. Phase content of iPP (T30G) from WAXD deconvolution as a function of the solidification pressure (from La Carrubba et al.[52]).

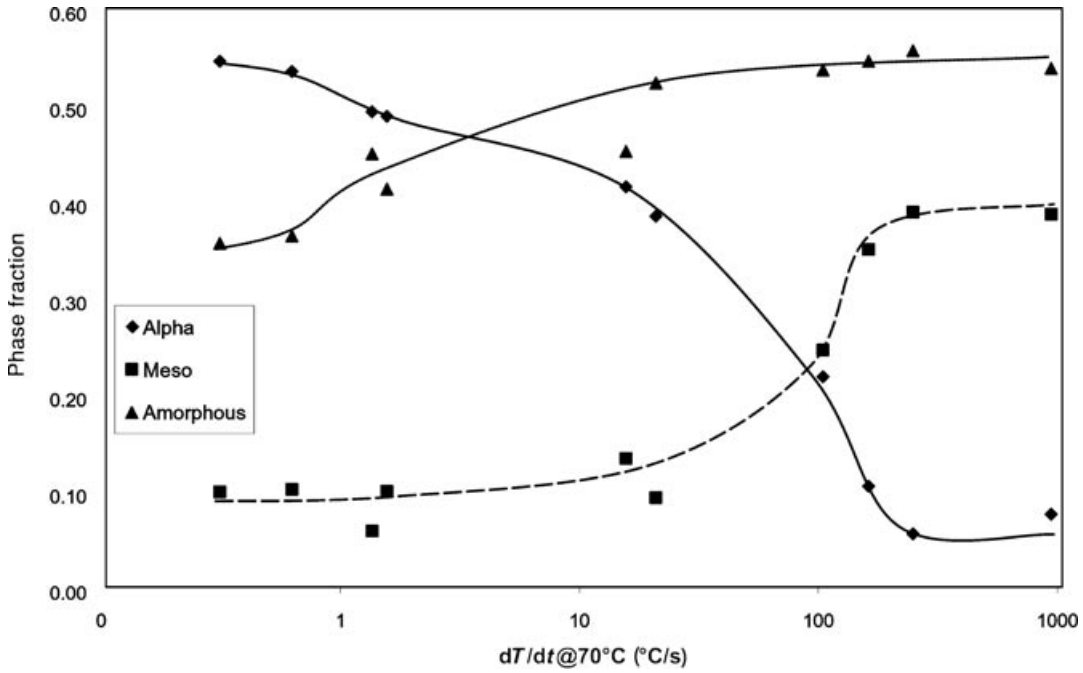

FIGURE 24. WAXD deconvolution of iPP (T30G) at 0.1 MPa, showing the α, mesomorphic, and amorphous phase relative content (from La Carrubba et al.[52]).

see how the decrease in the α phase with increasing the cooling rate is accompanied by an increase in the mesomorphic phase (Fig. 23). This observation is a further confirmation of the validity of the master curve approach to describe the behavior of iPP.[70]

Polyamide-6

In Fig. 25, plots of the density of PA6 as a function of depth (diaphragm 3.5 mm thick) for all solidification pressures used are shown. Three different zones can be identified. In the first zone, near the

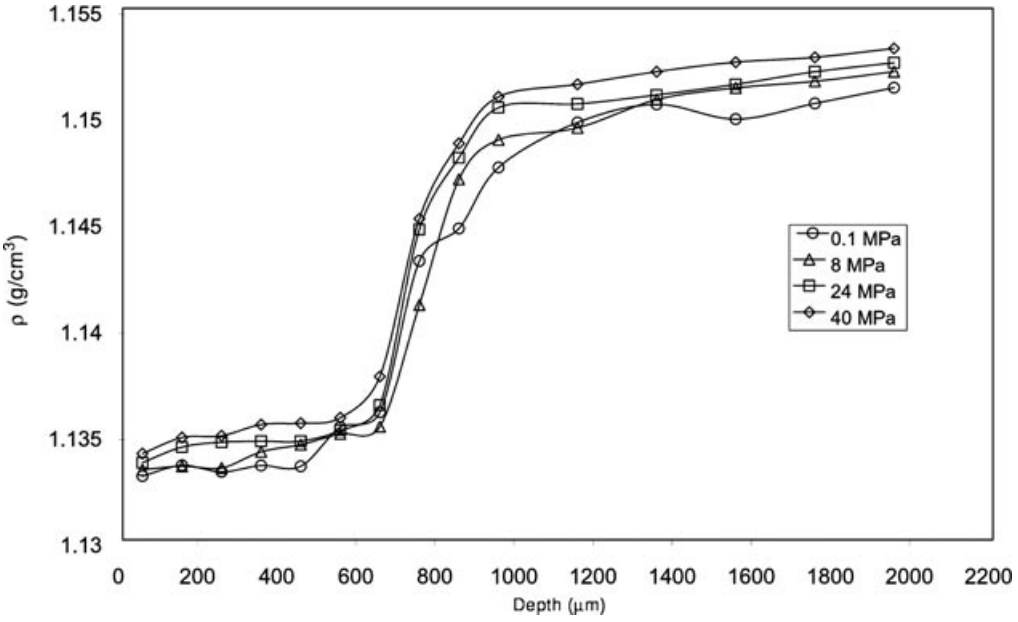

FIGURE 25. PA6 density depth profile for different pressures from 0.1 to 40 Mpa (from La Carrubba et al.[52]).

cooled wall, the density remains nearly constant up to a depth of around 700 μm. There is only a very small difference between the density of the samples crystallized at ambient pressure relative to those crystallized under higher pressure conditions. The recorded increase of density with increasing solidification pressure, however, is not negligible.

The second zone can be regarded as a "transition zone," denoting a zone where the most significant variation of density vs. depth takes place. This region is formed in the zone between 700 and 1000 μm and is independent of the solidification pressure. Finally, the third region, i.e. the "bulk," starts from a depth of approximately 1000 μm. This is the region where the density tends to level up to the center of the sample. The effect of solidification pressure on the density of the sample across this zone appears to be more pronounced than in the low-density region. An increase in pressure results in a larger increase in the final density. On the whole, the increase of density due to the increase of solidification pressure is of the same order of magnitude as the decrease of density observed in the case of iPP (discussed earlier). This evidence is in full agreement with the dilatometric results reported by He and Zoller[6] in 1994. Using a "GNOMIX confining fluid dilatometer," these authors found a 0.1% decrease of density of iPP measured at 10 MPa for samples crystallized at 10 and 100 MPa. However, they reported an increase of density of 0.3% in the case of PA66. It should be remembered that the cooling rate adopted during their experiments was very low (2.5°C/min) due to the intrinsic constraints imposed by the apparatus.

The same trend is observed if the density of PA6 is reported as a function of the cooling rate measured at 135°C,[45,52] as it can be observed by looking at the data in Fig. 26. The low-density plateau corresponds to the high cooling rate region, which starts at cooling rates above 10°C/s. This region spans over more than 1 order of magnitude in cooling rates, up to 250°C/s. The high-density plateau, on the other hand, covers nearly 1 order of magnitude in the cooling rate, moving from the lowest achieved rate during the experiment (1°C/s) to 7–8°C/s. As for the transition zone, it should be emphasized that it is located in a very narrow region, centered at a cooling rate of about 8–10°C/s. This cooling rate can be defined as a sort of "critical cooling rate," because small changes in the cooling rate around this value can bring about large structural and morphological variations and concomitant large variations in density. A very similar value of the critical cooling rate has already been found for a different PA6 some years ago. These are is in agreement with the results presented here.[31] The critical cooling rate corresponds to the so-called "crystallizability" value defined by Ziabicki several years ago.[72]

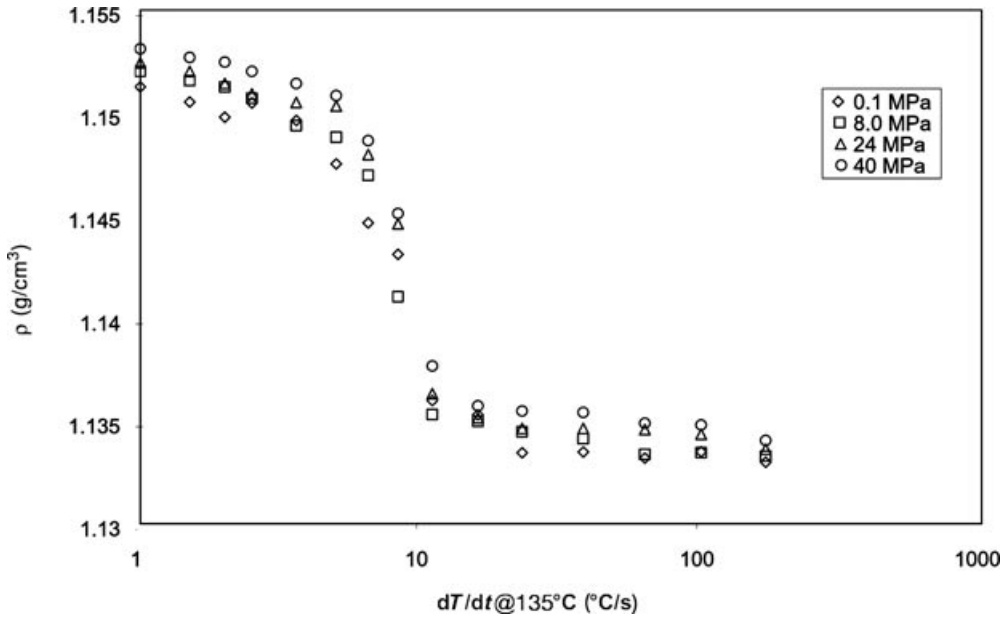

FIGURE 26. PA6 Density vs. cooling rate evaluated at 135°C for different pressures from 0.1 to 40 Mpa (from La Carrubba et al.[52]).

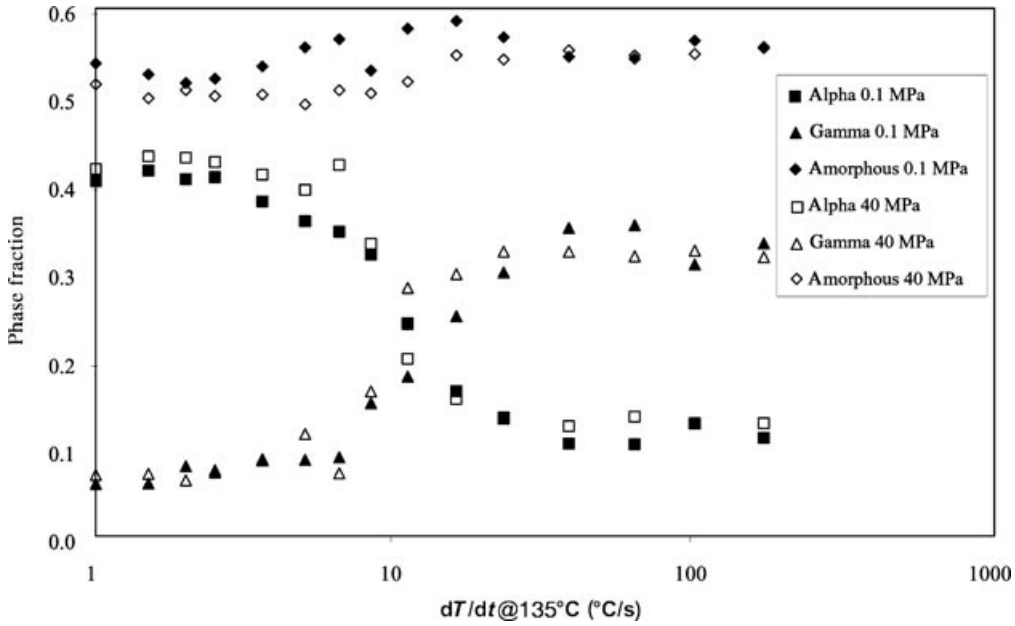

FIGURE 27. PA6 phase content from WAXD deconvolution at two different pressure values (indicated in the legend; from La Carrubba et al.[52]).

The results of the deconvolution of the WAXD data for PA6 samples are reported in Fig. 27. These show plots of phase distribution as a function of the cooling rate for samples crystallized at atmospheric pressure and at 40 MPa. It is easily noted that the phase content is in good agreement with density results shown in Fig. 26, with the α-phase drop located around 10°C/s. Moreover, the curves in Fig. 27 show that an increase in pressure corresponds to an increase of the α-phase content in the low cooling rate region (i.e., in the high α-phase content zone). This increase of the α phase is mainly compensated by a corresponding decrease of the amorphous phase content, whereas the variation of the γ-phase content is almost negligible. In any case, as already observed for the density data (Fig. 26), the variation in α-phase content is very small, and, therefore, the difference may be considered significant only changing the pressure from 0.1 MPa to 40 MPa.

Polyethyleneterephthalate

The high intrinsic brittleness of crystalline PET made it impossible to produce microtomed slices for measuring density. Consequently, to evaluate the influence of pressure on crystallization kinetics of PET, several microhardness measurements were performed, on samples crystallized under pressure, along a direction perpendicular to the quenched surface (see Fig. 8). A standard Vickers microindenter was used, using a load of 100 g applied for 6 s and a loading rate equal to 50 g/s. In this way, a complete mapping of the hardness values for the sample could be obtained. Microhardness value can be related to the crystallinity level of the sample, even though an accurate relationship between microhardness and crystallinity is quite complex, and it depends on the texture of the sample.[18,51,73]

Experimental results of the microhardness values taken at various depths for all solidification pressures are reported in Fig. 28. As in the case of iPP, the microhardness increases from the cooled surface to the bulk of the sample, because the internal layers of polymer are subjected to a less severe quenching. This reflects a similar change in the level of crystallinity.

As for dependence of crystallization on the pressure is concerned, PET displays the opposite behavior with respect to that of iPP (see the density data reported in Figs. 19–20). For PET, an increase in pressure corresponds to an increase of the microhardness. Phillips and Tseng[74] have found similar results on PET crystallized under pressures up to 200 MPa. They observed a reduction in the average spherulite size as pressure was increased. The effect was much greater than that observed in other studies on different polymers. A crystallinity level nearly double the one obtained at atmospheric pressure was obtained

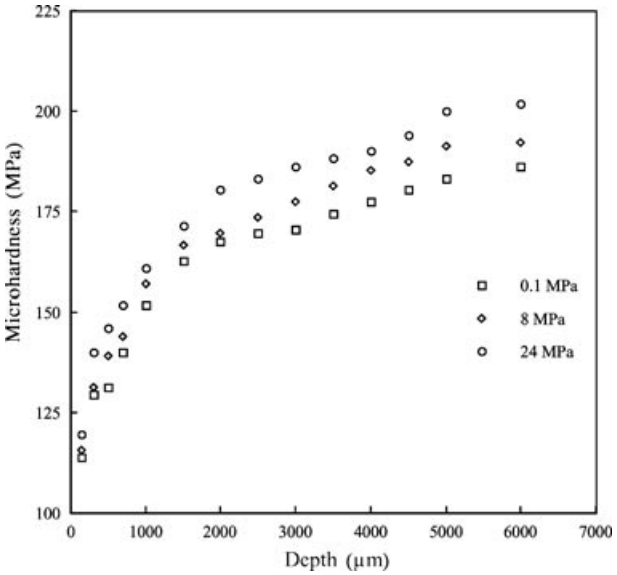

FIGURE 28. PET microhardness depth profile (diaphragm 3.5-mm thick) for different solidification pressures from 0.1 to 24 Mpa (from La Carrubba et al.[65]).

at a pressure of 150 MPa. It appears from their results that the increase of density with pressure is a direct consequence of the applied pressure during crystallization, because PET is a polymer with very rigid repeating units. This indicates that, possibly, molecular flexibility could be the key to understand the difference in behavior displayed by iPP and PET under pressure. Furthermore, the present results are in agreement with the experimental results presented by He and Zoller,[6] who found a significant increase of density with pressure for PET, in contrast with the decrease observed for iPP.

By using the "depth–cooling rate transformation function" for PET (see Fig. 9), the microhardness values can be plotted against the calculated cooling rate (measured at 170°C). The curves in Fig. 29 show that micro-hardness decreases when the cooling rate increases. Furthermore, at a constant cooling rate, the microhardness increases with pressure over the entire cooling rate range examined. Finally, the microhardness decreases almost linearly with the cooling rate (in a log scale) for all solidification pressures.

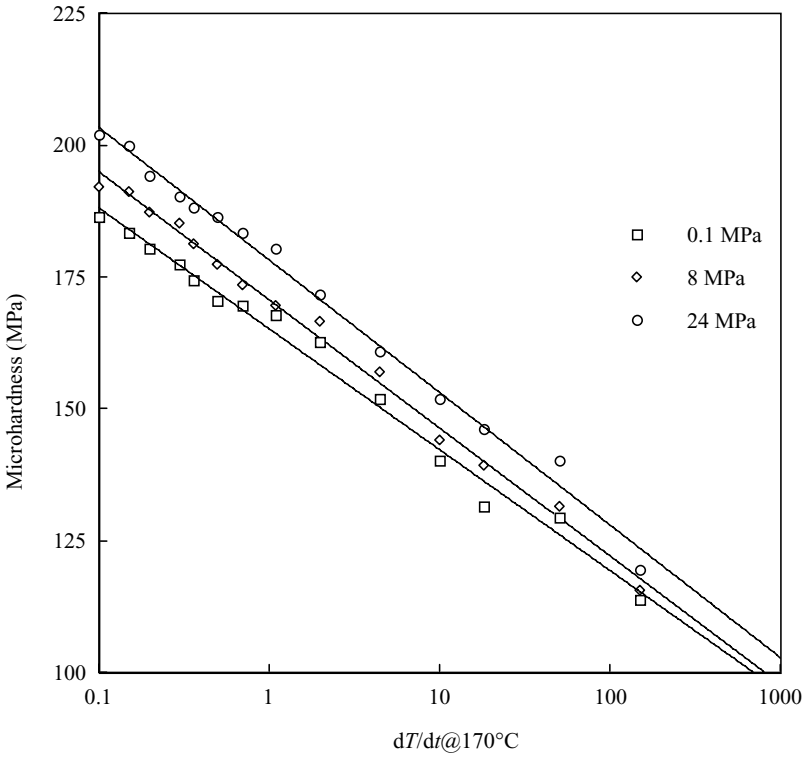

FIGURE 29. PET Microhardness vs. cooling rate evaluated at 170°C for different solidification pressures from 0.1 to 24 Mpa (from La Carrubba et al.[65]).

Comparison of the Crystallization Behavior under Pressure of iPP, PA6, and PET

A detailed explanation of the influence of pressure on the solidification of PA6 and PET compared with iPP has been presented elsewhere.[52]

For the scope of this review, it is sufficient to concentrate on the observed modification of crystallization kinetics on increasing the solidification pressure, elucidating the dependence on the applied pressure of both the glass transition (kinetic effect), and the melting temperature (thermodynamic effect). If the increase of melting temperature with pressure is larger than the increase of glass transition temperature, one should expect an increase in the degree of crystallinity with pressure, as it is observed for PA6 and PET. If the increase of the glass transition temperature with pressure (as reported for iPP[51,52]), on the other hand, is much larger than of the melting temperature, a significant slowing down of crystallization kinetics (i.e., of "crystallizability," see Ziabicki[72]) must be expected. The results outlined provide a confirmation of the hypothesis predicting a decrease of crystallinity upon increasing pressure for iPP as a "kinetic-dependent" phenomenon (as suggested also by Hieber[75]). This is because the major effect of an increase of the solidification pressure is the decrease of chain mobility (i.e., a decrease of free volume). In other words, this behavior strongly depends on a significant diffusion control over crystallization kinetics. Furthermore, the observed levelling off of the curves reporting density as a function of the cooling rate for increasing levels of pressure (Fig. 21) can be easily interpreted as a competition between a "kinetic" effect (related to the increase of the glass transition temperature with pressure) and a "thermodynamic" effect (due the increase of the melting temperature with pressure). In other words, upon increasing the solidification pressure, the resulting increase of the melting temperature becomes increasingly greater, hindering the effect of "quenching" related to the shift of the glass transition temperature. This competition eventually determines the observed levelling off of crystallinity (and density) with solidification pressure.

In the case of PA6 and PET, the "kinetic" effect due to pressure increase is less prominent, making the "thermodynamic" effect the prevailing factor responsible for an increase in density (and microhardness) with increasing the solidification pressure.

On the basis of the crystallization kinetic behavior of the polymers so far examined (iPP, PA6, PET), one could provide a "rule of thumb" or a zeroth approach for the description of polymer crystallization behavior under nonisothermal conditions. That is, the faster the crystallization kinetics (as in the case of iPP), the more prominent will be the "kinetic effect" induced by a pressure increase (a decrease of crystallinity). On the other hand, the slower the crystallization kinetics (as in the case of PET) the more prominent will be the "thermodynamic effect" of pressure (an increase of crystallinity when pressure increases).

Syndiotactic Polystyrene

As a final example, we report the effect of pressure on the crystallization behavior of syndiotactic polystyrene. In Fig. 18, the peculiar dependence of density on the cooling rate for sPS samples solidified at atmospheric pressure is shown. Upon solidification under pressure, the trend reported in Fig. 30 is obtained by converting the data for the variation of density with depth data via the "mapping function" shown in Fig. 9. For a diaphragm with thickness of 4.5 mm the following salient features are revealed:

(a) density always displays a minimum at all solidification pressures;
(b) an increase of pressure brings about a shift of the density minimum toward higher cooling rates;
(c) a saturation effect takes place, such that density differences among samples solidified at 12 and 40 MPa become negligible;
(d) the density of samples solidified under pressure is higher than that of samples solidified at atmospheric pressure up to cooling rates of 3°C/s, where an inversion takes place.

The aforementioned findings point to a dependence of the β-phase content on pressure, with a related increase in density in the low cooling rate zone. The lower density values observed at larger cooling rates can, therefore, be reasonably related to a different amount of α and/or amorphous phases.

These deductions are confirmed by the phase distribution under pressure shown in Fig. 31, where the phase content is reported as a function of the cooling rate at two different pressure levels, 0.1 MPa (already shown in Fig. 5) and 12 MPa. From these curves, it is clear that the effect of pressure is more pronounced in the low cooling rate region (0.3–3°C/s), where a significant increase of the β-phase content is

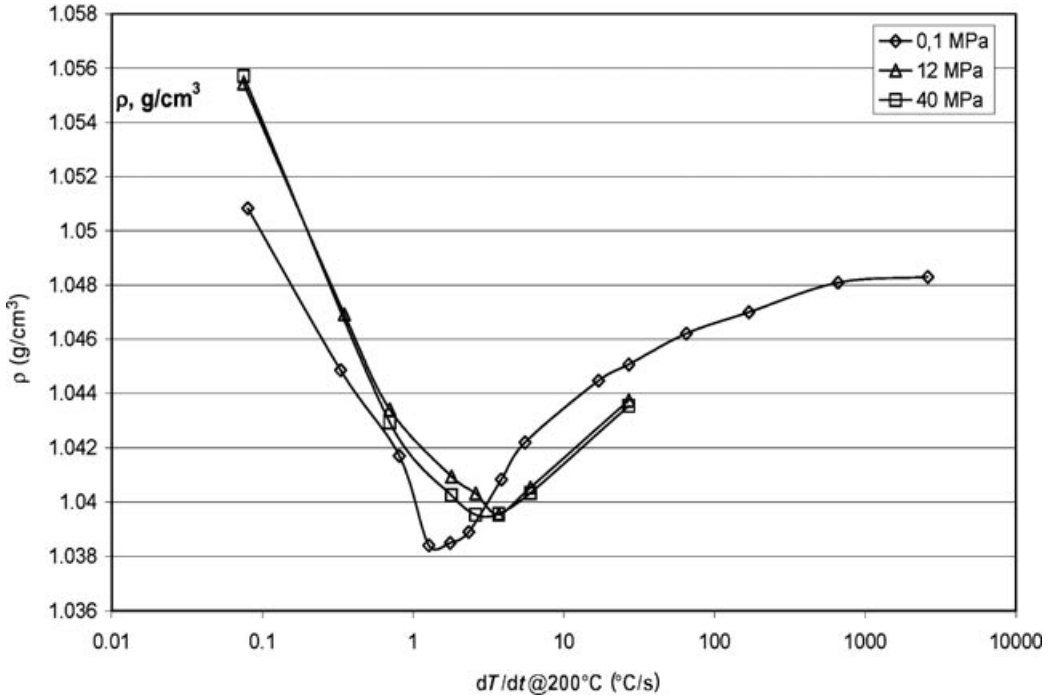

FIGURE 30. Density as a function of the cooling rate at three different pressure levels (0.1, 12, and 40 MPa) for syndiotactic polystyrene samples.

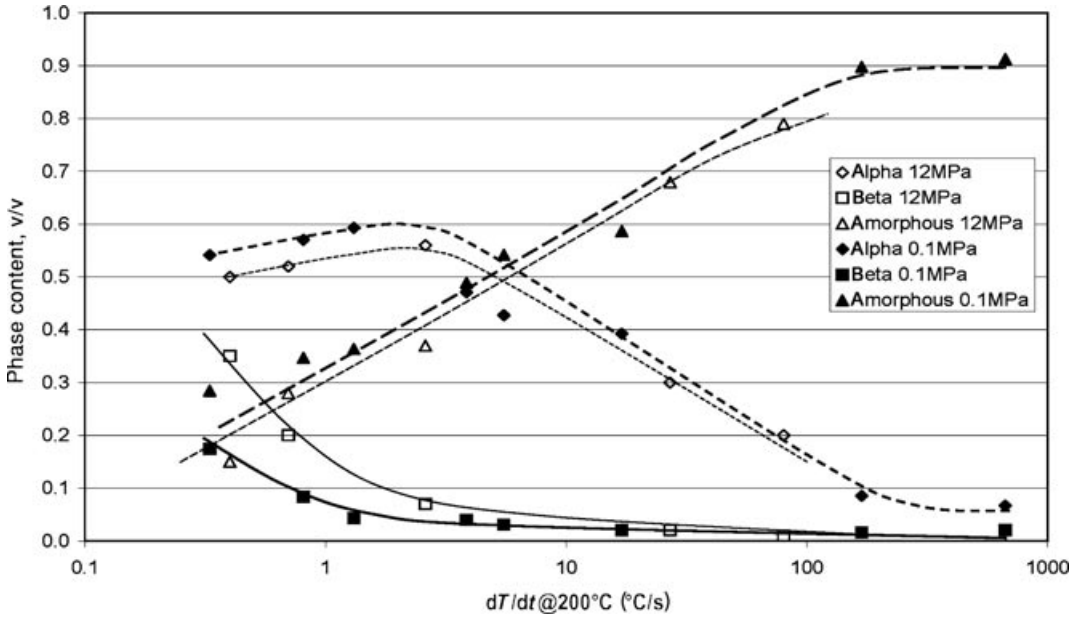

FIGURE 31. Phase distribution of sPS samples as a function of the cooling rate at 0.1 and 12 MPa.

observed upon increasing pressure. This relative increase occurs mainly at the expenses of the α-phase content, whereas the amorphous phase content is almost unaffected by the pressure increase.

Therefore, a pressure increase produces a larger β-phase content, but the amount becomes negligible at larger cooling rates relatively to the amount obtained for solidification at atmospheric pressure. This also explains the shift of density minimum toward larger cooling rates (taking place at a cooling rate where the amount of the β-phase tends to become negligible).

Concluding Remarks

An innovative experimental route has been evaluated to determine qualitatively the crystallization kinetics behavior of several semicrystalline polymers.

A scale of crystallization rates is suggested by this study that may be easily confirmed by a more accurate and detailed analysis of the crystallization kinetics based on the same data. In this sense, this experimental procedure establishes the basis for a complete description of the crystallization kinetics under processing conditions (high cooling rates and pressures), as it provides reliable data for semicrystalline polymers solidified under conditions comparable to those experienced in injection molding.

In particular, for iPP and PA6 an increase of the cooling rate at a constant solidification pressure is accompanied by a parallel decrease of the density and crystallinity. In PET samples, microhardness (linked to the crystalline phase content) decreases on increasing the cooling rate. Syndiotactic polystyrene, owing to the influence of the cooling rate on its complex polymorphic behavior, exhibits a minimum in the density vs. a cooling rate curve.

The influence of pressure on the final structure is deeply dependent on the peculiar behavior of each material. iPP exhibits a "negative dependence" of crystallization kinetics on pressure, because the final crystalline content (and density) tends to lower values on increasing pressure. In other words, the applied pressure acts as a "quenching factor" with respect to crystallization. PET and PA6 samples, on the other hand, exhibit a "positive dependence" of crystallization kinetics on pressure, since the final crystalline content becomes greater as pressure increases. In this case the pressure can be said to have an "antiquenching effect."

In sPS, an increase of pressure results in a shift of the minimum for the density vs. the cooling rate toward larger cooling rate values.

References

1. Ding, Z.; Spruiell, J. J Polym Sci, Part B:Polym Phys 1996, 34, 2783.
2. Eder, G.; Janeschitz-Kriegl, H. Material Science and Technology, vol. 18; Wiley–VCH Verlag GmbH, Germany: H.E.H. Meijer, 1997.
3. Brucato, V.; Piccarolo, S.; La Carrubba, V. Chem Eng Sci 2002, 57, 4129.
4. Leute, U.; Dollhopf, W.; Liska, E. Colloid Polym Sci 1976, 254(3), 237.
5. Zoller, P. J Appl Polym Sci 1979, 23(4), 1051.
6. He, J.; Zoller, P. J Polym Sci, Part B: Polym Phys 1994, 32(6), 1049.
7. Douillard, A.; Dumazet, Ph.; Chabert, B.; & Guillet, J. Polymer 1993, 34(8), 1702.
8. Fann, D. M.; Huang, S. K.; Lee, J. Y. Polym Eng Sci 1998, 38(2), 265.
9. Liangbin, L.; Huang, R.; Ai, L.; Fude, N.; Shiming, H.; Chunmei, W.; Yuemao, Z.; Dong W. Polymer 2000, 41, 6943.
10. Brucato, V.; De Santis, F.; Giannatasio, A.; Lamberti, G.; Titomanlio, G.; Macromol Symp 2002, 185, 181.
11. Lamberti, G.; De Santis, F.; Titomanlio, G.; Brucato, V. Appl Phys A 2004, 78, 895.
12. Strobl, G. The Physics of Polymers, Concepts for Understanding Their Structures and Behavior;, Springer-Verlag: New York, 1997.
13. Piccarolo, S. J Macromol Sci B 1992, 31(4), 501.
14. Piccarolo, S.; Saiu, M.; Brucato, V.; Titomanlio, G. J Appl Polym Sci 1992, 46, 625.
15. Choi, C.; White, J. L. Polym Eng Sci 2000, 40(3), 645.
16. Rotter, G.; Ishida, H. J Polym Sci, Part B: Polym Phys 1992, 30, 489.
17. Fu, Y.; Annis, B.; Boller, A.; Jin, Y.; Wunderlich, B. J Polym Sci, Part B: Polym Phys 1994, 32, 2289.
18. Piccarolo, S.; Brucato, V.; Kiflie, Z. Polym Eng Sci 2000, 40(6), 1263.
19. Wunderlich, B.; Arakawa, T. J Polym Sci, Part A: Polym Chem 1964, 2, 3697.
20. Geil, P. H.; Anderson, F. R.; Wunderlich, B.; Arakawa, T. J Polym Sci, Part A: Polym Chem 1964, 2, 3707.
21. Tchizmakov, M. B.; Kostantinopolskaja, M. B.; Zubov, Yu. A.; Bakeev, N. Ph.; Kotov, N. M.; Belov, G. P. Visokomol Soed A 1976, 18, 1121.
22. Wunderlich, B. Macromolecular Physics, Vol. 1; Academic Press: New York, 1973.
23. Wunderlich, B. Macromolecular Physics, Vol. 2; Academic Press: New York, 1976.
24. Wunderlich, B. Macromolecular Physics, Vol. 3; Academic Press: New York, 1980.

25. Wunderlich, B.; Davidson, T. J Polym Sci, Part A: Polym Chem 1969, 7, 2043.
26. Kovarskii, A. High-Pressure Chemistry and Physics of Polymers; CRC Press: Boca Raton, FL, 1994.
27. Goodfellow Catalogue. Goodfellow Cambridge Limited, 1996; p 318.
28. Alfonso, G. C.; Ziabicki, A. Coll Polym Sci 1995, 273, 317.
29. Ziabicki, A.; Alfonso, G. C. Coll Polym Sci 1994, 272, 1027.
30. Brucato, V.; Crippa, G.; Piccarolo, S.; Titomanlio, G. Polym Eng Sci 1991, 31, 1411.
31. Brucato, V.; Piccarolo, S.; Titomanlio, G. Int J Form Proc 1998, 1(1), 35.
32. Titomanlio, G.; Speranza, V.; Brucato, V. Int Polym Proc 1997, 12(1), 45.
33. Titomanlio, G.; Piccarolo, S.; Levati, G. J Appl Polym Sci 1988, 35, 1483.
34. Titomanlio, G.; Rallis, A.; Piccarolo, S. Polym Eng Sci 1988, 29, 209.
35. Isachenko, V. P.; Ossipova, V. A.; Sukomel, A. S. Heat Transfer; MIR: Moscow, 1987.
36. Carslaw, H. S.; Jaeger, J. C. Conduction of Heat in Solids; London: Oxford Science, 1986.
37. Bird, R. B.; Stewart, W. E.; Lightfoot, E. N. Transport Phenomena; Wiley: New York, 1960.
38. Ciofalo, M.; Di Piazza, I.; Brucato, V. Int J Heat Mass Transfer 1998, 42, 1157.
39. Piccarolo, S.; Alessi, S.; Brucato, V.; Titomanlio, G. In Proceedings of Crystallization of Polymers, a NATO Advanced Research Workshop, Mons 1992, 405, 475.
40. Piccarolo, S.; Brucato, V. In Proceeding of the PPS12-Annual Meeting, Sorrento, Italy, 1996, 663.
41. Brucato, V.; Foresta, T.; Piccarolo, S. In Proceedings of NUPHIMAT '96, Sophia-Antipolis, France, 1996, 125.
42. Brucato, V.; Piccarolo, S.; Titomanlio, G. Makromol Chem Macrom Symp 1993, 68, 245.
43. Brucato, V.; Piccarolo, S.; Titomanlio, G. In Proceeding of European Regional Meeting of the Polymer Processing Society, Palermo, Italy, 1991, p. 299.
44. Brucato, V.; Piccarolo, S.; Titomanlio, G. In Proceeding of European XI PPS meeting, Stuttgart, Germany, 1995, p. 530.
45. La Carrubba, V.; Piccarolo, S.; Brucato, V. J Polym Sci, Part B: Polym Phys 2007, 45, 2688.
46. Luikov, A. V. Heat and Mass Transfer; Moscow: Mir Publishers, 1980.
47. Brandrup, J.; Immergut, E. H. Polymer Handbook; Wiley: New York, 1989.
48. Van Krevelen, W. Properties of Polymers; Elsevier: Amsterdam, 1972.
49. Gobbe, G.; Bazin, M.; Gounot, J.; Dehay, G. J Polym Sci, Part B: Polym Phys 1988, 26, 857.
50. Brucato, V.; Piccarolo, S.; La Carrubba, V. Int Polym Proc 2000, 15(1), 103.
51. La Carrubba, V. PhD thesis, CUES, Salerno, Italy, 2001.
52. La Carrubba, V.; Brucato, V.; Piccarolo, S. J Polym Sci, Part B: Polym Phys 2002 40(1), 153.
53. La Carrubba, V.; Piccarolo, S.; Brucato, V. J Appl Polym Sci 2007, 104, 1358.
54. Nakamura, K.; Katayama, K.; Amano, T. J Appl Polym Sci 1973, 17, 1031.
55. Corradini, P.; Petraccone, V.; De Rosa, C.; Guerra, G. Macromolecules 1986, 19, 2699.
56. Martorana, A.; Piccarolo, S.; Scichilone, F. Macromol Chem Phys 1997, 198, 597.
57. Struik, L. C. E. Physical Ageing in Amorphous Polymers and Other Materials; Elsevier: Amsterdam, 1978
58. Gerardi, F.; Piccarolo, S.; Martorana, A.; Sapoundjieva, D. Macromol Chem Phys 1997, 198, 3979.
59. Martorana, A.; Piccarolo, S.; Sapoundjieva, D. Macromol Chem Phys 1999, 200, 531.
60. Sondergaard, K.; Minà, P.; Piccarolo, S. J Macromol Sci Phys 1997, B36(6), 733.
61. Guerra, G.; Vitagliano, V.; De Rosa, C.; Petraccone, V.; Corradini, P. Macromolecules 1990, 23, 1539.
62. Sorrentino, A.; Pantani, R.; Titomanlio, G. J Polym Sci, Part B: Polym Phys 2007, 45, 196.
63. De Rosa, C.; Guerra, G.; Petraccone, V.; Pirozzi, B. Macromolecules 1997, 30, 4147.
64. De Rosa, C.; Rapacciuolo, M.; Guerra, G.; Petraccone, V.; Corradini, P. Polymer 1992, 33, 1423.
65. La Carrubba, V.; Brucato, V.; Piccarolo, S. Macromol Symp 2002, 180, 43.
66. Cartier, L.; Okihara, T.; Lotz, B. Macromolecules 1998, 31, 3303.
67. Van Hooy-Corstjens, C. S. J.; Holhne, G. W. H.; Rastogi, S. Macromolecules 2005, 38, 1814.
68. Rastogi S. In Proceedings of the 12th Annual Meeting of the Polymer Processing Society, Sorrento, Italy, 1996, p. 649.
69. Rastogi, S.; Vegaa, J. F.; van Rutha, N. J. L.; Terry, A. E. Polymer 2006, 47(15), 5555.
70. La Carrubba, V.; Brucato, V.; Piccarolo, S. Polym Eng Sci 2000, 40(11), 2430.
71. La Carrubba, V.; Briatico-Vangosa, F.; Brucato, V.; Piccarolo, S. Polym Bull 2002, 49, 159.
72. Ziabicki A. Fundamentals of Fibre Formation; Wiley: London, 1976.
73. Kiflie, Z.; Piccarolo, S.; Brucato, V.; Balta'-Calleja, F. J. Polymer 2002, 43(16), 4487.
74. Phillips, P. J.; Tseng, H. T. Macromolecules 1989, 22, 1649.
75. Hieber, C. A. Int Polym Proc 1997, 12, 249.